LBL-13286

Lawrence Berkeley Laboratory
UNIVERSITY OF CALIFORNIA, BERKELEY

EARTH SCIENCES DIVISION

A STATISTICAL FRACTURE MECHANICS APPROACH TO THE STRENGTH OF BRITTLE ROCK

Joe Lawrence Ratigan
(Ph.D. thesis)

June 1981

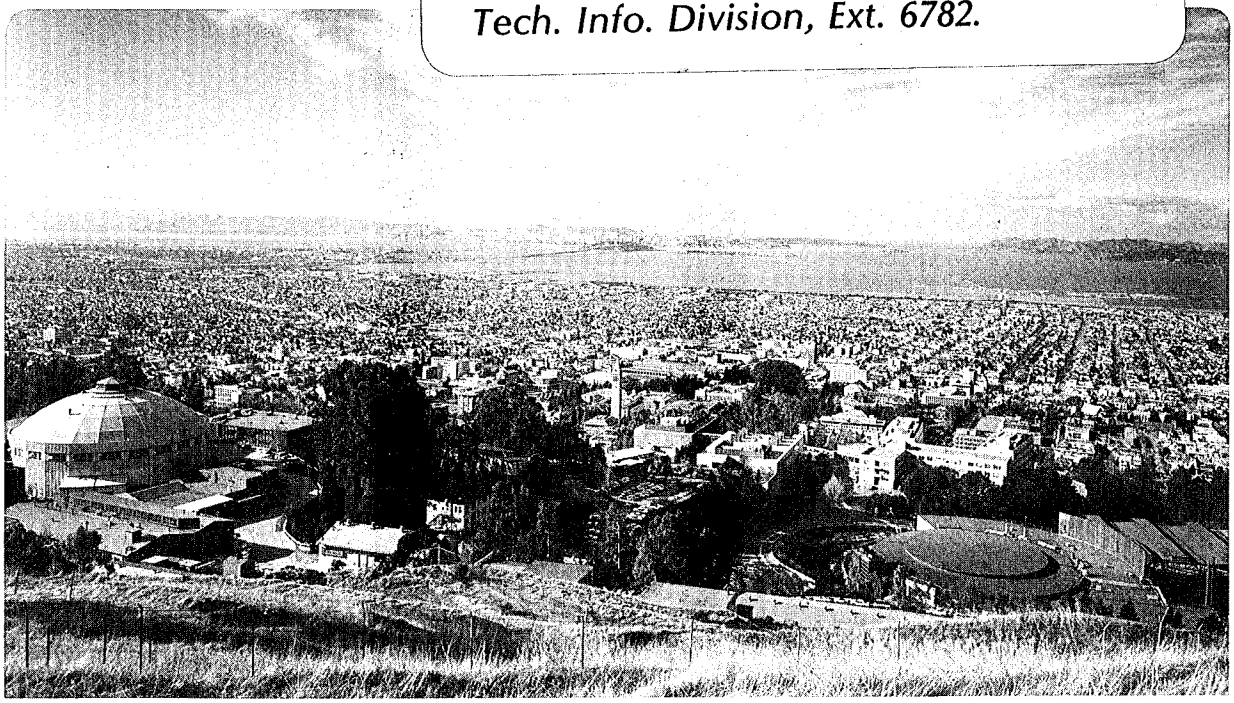

Prepared for the U.S. Department of Energy under Contract DE-AC03-76SF00098

LBL-13286

A STATISTICAL FRACTURE MECHANICS APPROACH TO THE STRENGTH OF BRITTLE ROCK

Joe Lawrence Ratigan

Ph.D. Thesis

June 1981

Lawrence Berkeley Laboratory and
Department of Civil Engineering
University of California, Berkeley
Berkeley, California 94720

This work was supported by the Assistant Secretary for Nuclear Energy, Office of Waste Isolation of the U.S. Department of Energy under contract DE-AC03-76SF00098. Funding for this project is administered by the Office of Nuclear Waste Isolation at Battelle Memorial Institute.

TABLE OF CONTENTS

ACKNOWLEDGEMENTS

This endeavor was made tractable through the support and encouragement of my wife, Dara and son, John. I am exceedingly grateful to and for both of them.

I wish to express appreciation to the members of my thesis committee for their assistance during the course of this research and for reviewing the manuscript. I also wish to thank Professor Richard E. Goodman for his unending enthusiasm and motivation; Professor Iain Finnie for so eloquently introducing me to the field of fracture mechanics and Professor Tor L. Brekke for exposing me to a seemingly infinite number of practical problems in rock mechanics.

To Jess Albino and Dr. Rick Nolting, I extend my sincere appreciation for detailing the intricacies of performing successful rock mechanics experiments at Berkeley. I also wish to thank Dr. Tom Doe for designing and/or supplying much of the equipment and instrumentation used in the testing performed in this research as well as for his able assistance in performing the hydraulic fracture experiments in the laboratory at Berkeley.

I am grateful to RE/SPEC Inc., the Lawrence Berkeley Laboratory Earth Sciences Division and the Jane Lewis Fellowship for providing financial assistance during my stay at Berkeley. The funds from RE/SPEC Inc. were made possible through the efforts of Dr. Paul F. Gnirk to whom I offer a very sincere *Thank You.*

A STATISTICAL FRACTURE MECHANICS APPROACH TO THE STRENGTH OF BRITTLE ROCK

Doctor of Philosophy Joe L. Ratigan Civil Engineering

R.E. Goodman
Chairman of Committee

ABSTRACT

Statistical fracture mechanics concepts used in the past for rock are critically reviewed and modifications are proposed which are warranted by (1) increased understanding of fracture provided by modern fracture mechanics and (2) laboratory test data both from the literature and from this research. Over 600 direct and indirect tension tests have been performed on three different rock types; Stripa Granite, Sierra White Granite and Carrara Marble. In several instances assumptions which are common in the literature were found to be invalid.

A three parameter statistical fracture mechanics model with Mode I critical strain energy release rate as the variant is presented. Methodologies for evaluating the parameters in this model as well as the more commonly employed two parameter models are discussed.

The experimental results and analysis of this research indicate that surfacially distributed flaws, rather than volumetrically distributed flaws are responsible for rupture in many testing situations. For several of the rock types tested, anisotropy (both in apparent tensile strength and size effect) precludes the use of contemporary statistical fracture mechanics models.

CHAPTER 1

INTRODUCTION

In the majority of rock mechanics problems, the engineer is seldom concerned with the tensile strength of intact rock, for the inherent discontinuities are the predominant structural component that usually determines the strength of the rock mass. However, there are a limited number of important situations wherein the knowledge of the apparent tensile strength of intact rock is of fundamental importance. For example, a knowledge of the apparent tensile strength in a hydraulic fracture experiment for the determination of in situ stress is fundamentally necessary if the state of stress is to be determined from the initiation of the hydraulically induced fracture. In certain underground situations, the apparent tensile strength of intact rock beams defined by jointing or bedding planes is important in determining required rock bolting. Proposed high technology uses of underground cavities such as LPG storage require a knowledge of apparent tensile strength, particularly as it relates to cyclic loading and potential fatigue failure.

When intact rock samples are taken into the laboratory and tested to determine tensile strength, three observations are invariably made.

(1) The apparent tensile strength depends upon the sample size (the larger the specimen, the smaller the strength)

(2) The apparent tensile strength depends upon the type of test being performed.

(3) With any given test and specimen size, a scatter (usually skewed) about the mean is obtained.

The first dilemma (commonly referred to as the *size effect)* is also observed with respect to compressive strength and an apparent Young's Modulus, although to a lesser extent than with tensile strength (*e.g.*, Heuze (1980)). However, the observation has

prompted many investigators to recognize that tensile strength of brittle rock is not a material property (*e.g.*, Hudson and Fairhurst (1969)). The second observation noted above has been brushed away by using different names to refer to the strength observed in different tests. For example, the apparent tensile strength in bending is referred to as the Modulus of Rupture. The tensile strength determined by indirect tension tests is often referred to with an adjective taken from the test; for example, the Brazilian tensile strength or the split cylinder tensile strength. The third observation above is often totally neglected in the reporting of test results. Scatter about the mean is often attributed to testing methodology and/or sample inhomogeniety. Thus, more often than not, the only result of the tensile testing may be the mean without the standard deviation or any of the other statistical moments. A premise of this Thesis and statistical fracture mechanics for that matter, is that all three of the observations above are consistent with the behavior of brittle materials.

In the classical continuum concept of strength, none of the observations noted above could be attributed to the inherent behavior of the material, but rather must be attributed to the testing methodology and/or the sample inhomogeniety. The probabilistic concept of the strength of brittle rock on the other hand is an integral concept rather than a differential concept which involves the geometry and volume of the specimen, the spatial stress distribution, and the distribution and strength of the failure inducing flaws within the specimen.

The purpose of this Thesis is to critically evaluate statistical fracture mechanics concepts and models used in the past for rock and to propose modifications which are warranted by (1) increased understanding of fracture provided by modern fracture mechanics and (2) laboratory test data both from the literature and from this research. With regard to the latter, over 600 direct and indirect tension tests have been performed during the course of this research on three different rock types; Stripa Granite, Sierra White Granite and Carrara Marble. Descriptions of these rock types are given in Appendix A. Various tests were specifically designed to evaluate the validity of major assumptions made in the past in

applying statistical fracture mechanics concepts to rock. In several instances, assumptions which have become common in the literature were found to be invalid.

In Chapter 2 of this Thesis, statistical fracture mechanics models used in the past are reviewed. Potential modifications to the commonly used models are presented in Chapter 3 including those warranted by test data appearing in the literature as well as several of the modifications necessary to analyze the *size effect* in compression. Methodologies for determining parameters for various statistical fracture mechanics models are presented in Chapter 4. In Chapter 5, the design of the tension tests performed during this research is given. Experimental data obtained during the research is presented in Chapter 6 for the three rock types. In Chapter 7, it is demonstrated that a statistical fracture mechanics model dictated by one test can be used to predict the strength in an entirely different test of significantly different scale. The conclusions and recommendations of this research are presented in Chapter 8.

CHAPTER 2

STATISTICAL FRACTURE MECHANICS

At the heart of statistical fracture mechanics is the supposition that materials inherently contain defects which eventually lead to structural collapse under increasing load. The concept of flaws or defects within materials was first popularized by Griffith (1921) in his formulation of a fracture criterion supposing flat elliptical flaws. Statistical fracture mechanics differs from a *Griffith type* criterion in that one hypothesizes at the onset that the flaws need not be geometrically uniform nor need they possess uniform strength. In geological materials, flaws or defects need not necessarily be physical voids, but may well be *soft* minerals in contact with significantly *stiffer* minerals (Brace (1964)). In this context, the softer minerals act much as if they were not present under the application of load. If one were able to establish the geometry of the failure inducing flaws, general statistical fracture criterion could be established for virtually any multiaxial stress state. Although this concept is discussed in Chapter 3, the geometry of the failure inducing defects will be considered to be flat for the remaining portions of this Thesis.

The formulation of a statistical fracture criterion requires the specification of both *global* and *local* failure criteria. The terms global and local are used rather loosly; however, they will become more obvious in later portions of this chapter. The global failure criterion is that which dictates the total collapse of the structure. The local failure criterion relates to the variant (in the statistical sense) which characterizes the failure of an individual material defect.

Throughout this Thesis, material response to load shall be assumed to be brittle. In other words, release of strain energy shall be assumed to occur only through rupture or fracture of the specimen. Brittle response is typically defined in the laboratory by the

observation of linear deformation response to load. However, this methodology may be misleading as shown in Chapters 5 and 7.

Three further assumptions will be made in this Thesis in the development of a statistical fracture criterion. Firstly, material defects shall be assumed to be present in large numbers. This is a necessary assumption in extreme value statistics (Gumbel (1958)). A quantification of *large* has been attempted by Jayatilaka and Trustrum (1977) who show that large may well imply 100 to 1000 defects within the specimen. The second assumption is that the material defects shall be isotropically distributed (Weibull (1939b)). This latter assumption appears to have been exclusively adopted in the rock mechanics literature involving applications of statistical fracture mechanics models. Experimental data presented in this Thesis indicates that this assumption is inappropriate for some rocks. The third assumption is that defects do not interact with one another. This assumption allows the use of continuum concepts for determining stress states in linear elastic materials.

Statistical fracture mechanics is intimately related to extreme value statistics. For a detailed treatment of extreme value statistics the reader is referred to Gumbel (1958) or to Benjamin and Cornell (1970) for a less detailed overview.

2.1 GLOBAL FAILURE CRITERION

Global failure criteria for statistical fracture mechanics models essentially relate to the quantity of material defects which must fail prior to collapse of the specimen. The options available are, of course, infinite. However, one can categorize global criteria into two classes, *viz*;

(1) Single defect criteria
(2) Multiple defect criteria.

The single defect criteria have been termed *Weakest Link Models* (Weibull (1939a)), for the collapse of the specimen depends only on the failure of a single link in a series structure of links. The Weakest Link Theory was popularized by Weibull in two papers in

1939 (Weibull (1939a), (1939b))[1] and has received considerable attention in the literature (Finnie (1977)).

Multiple defect criteria can best be understood by again referring to the chain analogy. These criteria invariably involve links in parallel, series of links in parallel, or some other combinations of parallel and series structures (*e.g.*, Wijk *et al* (1978)). Although the multiple defect criteria have received much less attention in the literature, the potential uses in progressive failure of materials by microcracking appears promising (*e.g.*, McClintock and Mayson (1976), McClintock (1977)).

The appropriateness of a single or multiple defect criterion is difficult to assess *a priori.* However, microcracking (indicative of the potential need for a multiple defect criterion) may be qualitatively assessed in the laboratory by means of the microseismic or acoustic emission techniques (Hardy and Leighton (1977), (1980)). This technique will be further discussed in Chapter 5.

Throughout this Thesis, the single defect or Weakest Link Model shall be assumed. Excellent treatises of the Weakest Link Theories are available in the literature (*e.g.*, Weibull (1939a), Freundenthal (1968)) and only the essential characteristics will be repeated here.

If we define the probability of failure of link i as f_i, then the survival probability P_s of a series structure of N such links is;

$$\begin{aligned} P_s &= (1-f_1)\ (1-f_2)\ \cdots\ (1-f_N) \\ &= \prod_{i=1}^{N}(1-f_i) \\ &= e^{\left[\ln \prod_{i=1}^{N}(1-f_i)\right]} \end{aligned} \tag{2-1}$$

[1] Although Weibull did not use the terminology "weakest link", he nonetheless presented the mathematical form which is known as the weakest link.

$$= e^{\left[\sum_{i=1}^{N} \ln (1-f_i)\right]}$$

If we further use the approximation $\ln(1+f_i) = f_i$ (implying f_i small) and assume that there is a sufficiently large number of flaws so as to replace the summation with an integral, we are led to;

$$P_s = e^{\left[-\int_R n(\sigma)\, dR\right]}$$

$$= 1 - P_f \tag{2-2}$$

where:

R	=	the geometric domain of the structure where defects reside
$n(\sigma)$	=	material function (number of flaws per unit region with strength $< \sigma$)
σ	=	stress (tension positive)
P_f	=	probability of failure.

The geometric domain, R, may be considered to be composed of the specimen volume as well as the free surfaces of the specimen. As will be shown in the next section, this multiple domain concept also allows for multiple $n(\sigma)$ functions; one for the volume and one for the free surfaces. If a material fails typically from a single pre-existing defect, Equation (2-2) is exact. However, empiricism will be introduced in the specification of $n(\sigma)$, the local failure criterion.

Weibull defined a term B, which he referred to as the *risk of rupture,* where:

$$B = \int_R n(\sigma)\, dR \tag{2-3}$$

For the remainder of this Thesis, the terminology *cumulative failure probability,* G, shall be used rather than the *probability of failure,* P_f, in order to be consistent with the literature. Some minor deviations in terminology and mathematical symbols exist between

Weibull's original work and the definitions and derivations in the next section of this chapter. The deviations are made for clarification.

2.2 LOCAL FAILURE CRITERION

The function $n(\sigma)$ may be determined in the laboratory for a specific test (Evans and Jones (1978)). This methodology will not be adopted, however, due to the lack of generality. Weibull (1939b) proposed a functional form for uniaxial tension;

$$n(\sigma) = \begin{cases} \left[\dfrac{x(\sigma) - x_u}{x_o} \right]^m & x(\sigma) > x_u \\ 0 & x(\sigma) \leqslant x_u \end{cases} \tag{2-4}$$

where:

x = some suitable function of stress

x_u = the value of x below which rupture does not occur

x_o = scaling constant

m = Weibull Modulus.

Weibull stated that the region R, could well be both a volumetric region in addition to a free surface region, so that in the general case, the risk of rupture can be stated as;

$$B = \int_S n_S(\sigma)\, dS + \int_V n_V(\sigma)\, dV \tag{2-5}$$

where:

$$n_S(\sigma) = \left[\frac{x(\sigma) - x_{u_S}}{x_{o_S}} \right]^{m_S}$$

$$n_V(\sigma) = \left[\frac{x(\sigma) - x_{u_V}}{x_{o_V}} \right]^{m_V}$$

Weibull's Theory is typically mis-stated in the literature as;

$$T_a\, V^{\frac{1}{m}} = \text{constant} \tag{2-6}$$

where:

T_a = apparent tensile strength.

Equation (2-6) is a specific form of Weibull's theory which only arises following the assumptions that (1) $x_u = 0$ and (2) $n_S(\sigma) = 0$. Both of these assumptions must be verified in the laboratory before being discarded or adopted.

Weibull selected the function $x(\sigma)$ to be the tensile stress normal to the material defect or flaw. Further, in much of Weibull's original work, he took $n_S(\sigma)$ to be negligible. Thus, Equation (2-6) becomes;

$$B = \int_V \left[\frac{\sigma - \sigma_u}{\sigma_o} \right]^m dV \tag{2-7}$$

This is popularly referred to as the Weibull three parameter model. When σ_u is equal to zero, the more commonly encountered two parameter Weibull model is obtained.

The mean apparent tensile strength for the Weibull three parameter model of Equation (2-7) can be shown to be (Weibull (1939a)):

$$\bar{T}_a = \sigma_u + \int_{\sigma_u}^{\infty} e^{-B} dT_a \tag{2-8}$$

All defects oriented such that a tensile stress is normal to the plane of the defect contribute to the risk of rupture, B. In this regard, the original derivation of B by Weibull is incomplete. For a uniaxial stress state, σ, the stress on the plane of a defect, σ_n with a normal at an angle ϕ, to σ is;

$$\sigma_n = \sigma \cos^2(\phi) \tag{2-9}$$

Integrating over the domain of ϕ for volumetrically distributed flaws results in a risk of rupture (for a three parameter model):

$$B = \int_V \int_{-\frac{\pi}{2}}^{\frac{\pi}{2}} \left[\frac{\sigma_n - \sigma_u}{\sigma_o} \right]^m d\phi \, dV \tag{2-10}$$

If $\sigma_u = 0$, the error is not important, for the constant σ_o is merely modified appropriately. However, any physical significance attached to σ_o would also have to be appropriately modified.

In a multiaxial stress field, the stress normal to a defect can be stated as;

$$\sigma_n = \sigma_1 n_1^2 + \sigma_2 n_2^2 + \sigma_3 n_3^2 \tag{2-11}$$

where;

n_1, n_2, n_3 = direction cosines

$\sigma_1, \sigma_2, \sigma_3$ = principal stresses.

The risk of rupture in the case of volumetrically distributed flaws is obtained by integrating over not only the volume, but also over all geometrically possible flaw orientations (see Figure 2-1).

$$B = \int_V \left[\int_{-\frac{\pi}{2}}^{\frac{\pi}{2}} \int_{-\frac{\pi}{2}}^{\frac{\pi}{2}} \frac{F \cos(\phi)\, d\phi\, d\psi}{2\pi} \right] dV \tag{2-12}$$

where:

$$F = \begin{cases} \left[\dfrac{\sigma_n - \sigma_u}{\sigma_o} \right]^m & \sigma_n > \sigma_u \\ 0 & \sigma_n \leqslant \sigma_u \end{cases}$$

$$\sigma_n = \left[\sigma_1 \cos^2(\psi) + \sigma_2 \sin^2(\psi)\right] \cos^2(\phi) + \sigma_3 \sin^2(\phi)$$

Note that the term 2π is included to "normalize" the magnitude of possible orientations (i.e., 2π = the surface area of a hemisphere).

Vardar and Finnie (1975) stated that Weibull's Theory suffered from the limitation that F did not reduce to a function of $\sigma_1 - \sigma_u$ when $\sigma_2 = \sigma_3 = 0$. However, as was shown, Equation (2-7) is incorrect. Thus, there is no reason why the multiaxial three parameter model should reduce to a form comparable to Equation (2-7).

CHAPTER 3

EXTENSIONS OF THE STATISTICAL FRACTURE MECHANICS MODELS

Chronologically, Weibull's Weakest Link Theory[1] development preceeded the development of modern fracture mechanics. When Weibull presented his formulation of a statistical fracture mechanics model, he implicity hypothesized that instantaneous propagation of a defect or flaw was dependent only on the tensile stress normal to the plane of the defect. In this same regard, defects were assumed to be insensitive to shear.

With the exception of Griffith's work (which lay dormant for some years) modern fracture mechanics did not experience a genesis that resulted in the present state-of-the-art until about 1950. Thus, there exists a significant chronological (and to some extent a technological) difference between Weibull's work and that of modern fracture mechanics.

In this chapter, potential extensions of Weibull's Theory are presented. Some of the extensions will be adopted in later chapters of this Thesis; others are presented because of the promise that they offer for future research efforts. Several of the extensions presented herein have appeared elsewhere in the literature and the reader will be referred to the more detailed treatises where appropriate.

3.1 STRAIN ENERGY FORMULATION

Following the initial work of Griffith (1921, 1924), Irwin (1948) presented the concept that the initiation of fracture propagation depended upon the critical strain energy release rate, G, in concert with a material property, G_c. If G is below G_c, propagation can not occur. This concept is one of the keystones of modern fracture mechanics. The determination of the strain energy release rate has been simplified for linear and nonlinear

[1]Henceforth, we shall refer to Weibull's Weakest Link Theory as Weibull's Theory.

materials in certain cases by Rice (1968) with his formulation of the J integral.

One unfortunate disadvantage of the strain energy release rate formulation is that one must be able to define the geometry of the crack in order to calculate the strain energy release rate associated with an arbitrary stress field. Statistical fracture mechanics was developed for those cases where we are *unable* to define the geometry of the defect. Although defect shapes may be assumed (*e.g.*, Evans (1978)), some physical verification must be established.

If we assume that a material contains flat, non-interacting cracks, the critical strain energy release rate associated with Mode I fracture can be shown to be;

$$G = k\,\sigma^2 \tag{3-1}$$

where:

k = a proportionality constant

σ = the tensile stress normal to the crack.

Using Equation (3-1), we may redefine Weibull's risk of rupture term $n(\sigma)$ as

$$n(\sigma) = \begin{cases} \left[\dfrac{G - G_u}{G_o}\right]^{\alpha} & G > G_u \\ 0 & G \leqslant G_u \end{cases} \tag{3-2}$$

where:

G = $\sigma_n^{\,2}$

G_u = threshold strain energy release rate

G_o = scaling constant.

Note that when $G_u = 0$, $\alpha = \dfrac{m}{2}$. We have introduced the terminology, α so that it is not confused with the Weibull Modulus, m, which appears so profusly in the literature. Further, the use of the term α is consistent with Freundenthal (1968) who presents a form similar to Equation (3-2) for $G_u = 0$. Equation (3-2) will be employed in the majority of

remaining chapters of this Thesis.

The mean apparent tensile strength for the three parameter model of Equation (3-2) can be shown to be;

$$\bar{T}_a = G_u^{1/2} + \int_{G_u^{1/2}}^{\infty} e^{-B} dT_a \tag{3-3}$$

3.2 COMPRESSION

A *size effect* with respect to rock compressive strength has been recognized (*e.g.*, Pratt *et al* (1972), Heuze(1980)). However, a mechanistic explanation has not been presented which satisfies all of the rock mechanics community. Statistical fracture mechanics models are typically inadequate for explaining size effects in compression for two reasons, *viz*;

(1) Defect failure criteria (referred to as local failure criteria in this Thesis) typically assume flat planar cracks which are insensitive to compression or shear regardless of defect orientation with respect to the applied stress.

(2) Most statistical fracture mechanics models assume a weakest link model (single defect global failure criterion) which is not representative of the physical conditions in the usual laboratory compression testing of rock (Baecher, 1970)).

Investigators of brittle inoculated iron (Cornet and Grassi (1955)) recognized that defects in these materials were not planar. In this regard, Cornet and Grassi formulated a deterministic fracture mechanics criterion based on the realization that compressive stresses in the plane of the largest dimension of an elliptical crack induced a tension proportional to the ratio of the length of minor axis to the length of the major axis of the elliptical defect. Thus, these investigators arrived at a functional form of a fracture criterion equivalent to a generalized Mohr-Coulomb criterion without introducing any concept of *internal friction.*

Vardar (1975) introduced this notion into a local failure criterion of a weakest link model in an effort to evaluate *how flat* a defect must be in order to render the Weibull

Theory accurate. Vardar redefined the tensile stress normal to the plane of a defect as;

$$\sigma_\eta = \sigma_n - \beta\hat{\sigma}_n \tag{3-4}$$

where:

σ_η = equivalent tensile normal stress at the defect tip

σ_n = stress normal to the defect plane

$\hat{\sigma}_n$ = normal stress in the plane of the defect

β = proportionality constant (ratio of minor to major axis in the case of an elliptical crack).

When evaluating the risk of rupture using Equation (3-4) additional integrations are necessary to account for the geometric possibilities of flaw orientations at any location on the unit sphere in the principal stress space (Vardar (1975)). Employing Vardar's concept, the risk of rupture with $G_u = 0$ for uniaxial tension can be equated to that for a triaxial test with $(\sigma_1 = \sigma_2 \geqslant \sigma_3)$. The resulting fracture criteria are illustrated in Figure 3-1 for $m = 5$ and $m = 15$ and for various values of β. Similarly, the biaxial fracture criterion $(\sigma_2 = 0)$ is illustrated in Figure 3-2. It is of qualitative interest to note that for m small, the fracture criterion is functionally similar to the von Mises distortional energy criterion $(\beta = 1)$ or the Drucker-Prager $(\beta > 1)$. As the magnitude of m increases, the biaxial fracture criterion functionally approaches a Tresca $(\beta = 1)$ or Mohr-Coulomb $(\beta > 1)$ criterion. Thus, the significance of the intermediate principal stress decreases for m large and *corners* in the fracture envelope begin to form.

The development of Figures 3-1 and 3-2 implicitly assumes constant surface area and volume in addition to the obvious requirement of geometrically similar stress fields.

The fracture criterion presented can not be directly applied to the compressive strength of rock. Since these figures were constructed with a weakest link global criterion, they are only applicable at the point of failure of the first defect. This point in the loading

history of a specimen is commonly referred to as the point of dilation initiation (Brace (1964)). Compressive failure of rock in conventional laboratory testing occurs from the interconnecting of individual defect failures to a final *faulting*. While the initiation of dilation can well be expected to be represented as an extreme value problem (in the statistical sense) the final faulting can not (Baecher (1970)). Nonetheless, the author feels that further research into the defect structure and local failure criterion may lead to an increased understanding of size effects in compression.

CHAPTER 4

EVALUATION OF MODEL PARAMETERS

Before presenting specific methodologies for evaluating the parameters of a statistical fracture mechanics model, some of the salient features of the mathematical forms will be reviewed. A more detailed discussion of some of what follows is given by Weibull (1939b).

For any tension test the stress state in the specimen can be stated as;

$$\sigma(x_i) = T_a \, f(x_i) \qquad i = 1,2,3 \tag{4-1}$$

where:

x_i = spatial coordinate

$f(x_i)$ = function whose value is $\leqslant 1$ in the domain where $\sigma(x_i) > 0$.

Using Equation (4-1), the risk of rupture for a two parameter model can be stated as;

$$B = T_a{}^m \left[C_S + C_V \right] \tag{4-2}$$

where:

C_S = a constant arising from integration over the surface

C_V = a constant arising from integration over the volume.

Thus, the cumulative probability of failure, $G(T_a)$ can be stated as;

$$G(T_a) = 1 - e^{\left[-T_a{}^m C\right]} \tag{4-3}$$

where:

C = a constant.

Rearranging and taking logarithms twice;

$$\ln \ln \left[\frac{1}{1 - G(T_a)} \right] = m \ln \left[T_a C^{\frac{1}{m}} \right] \tag{4-4}$$

$$= m \ln \left(\frac{T_a}{A_1} \right) + \ln \left(\frac{C}{A_2} \right)$$

In Equation (4-4), A_1 and A_2 are constants whose magnitude is unity and whose dimensions agree with those of the numerator. The significance of Equation (4-4) is that a space has been found wherein Equation (4-3) is a straight line with slope m.

For a two parameter model, the relationship between apparent tensile strength between any two tensile tests (or the same test at different volumes (or surface area)) can be obtained by equating the risk of rupture at the same failure probability. For example, the modal value of apparent tensile strength occurs at G = 0.5 or;

$$-B = \ln(0.5) \tag{4-5}$$

4.1 TWO PARAMETER MODELS

A multitude of methods exists for determining the parameters for a two parameter model whether the variant is stress or strain energy (*e.g.*, Robinson (1970), Robinson and Finnie (1969)). However, we may categorize all of the methods into two general classes, *viz*;

Class I : Methods relying on the frequency histogram of measured strengths or statistical moments of the histogram for a given test series.

Class II : Methods relying on the relationship between statistical moments (usually, the mean) between two or more test series.

Despite the extreme difficulty in determining the histogram accurately (Freundenthal (1968)), methods in Class I above appear to have received the greatest application in the literature. In the literature review for this Thesis, the Author never encountered a publica-

tion wherein methods from both classes were employed even though sufficient data often existed (*e.g.*, Lundborg (1967), Sundae (1974)).

The most popular method in Class I is to employ the formulation of Equation (4-4) (*e.g.*, Weibull (1939a), (1939b), Vardar and Finnie (1975)). In this manner, the experimental data (strengths) are ranked in ascending order and assigned a cumulative probability of failure G as;

$$G = \frac{j}{N+1} \tag{4-6}$$

where:

j = the rank position

N = the number of tests.

Robinson (1970) has shown that other definitions of G may be more appropriate. However, we shall use the previous definition throughout this Thesis. Several important properties of this methodology (most of which are discussed by Weibull (1939b)) deserve attention.

If the plot of the experimental data deviates from linearity, the material is not well represented with a two parameter model. If the curvature is concave downward, a three parameter model is suggested. Other potential material features can be identified in this functional space; for example, anisotropy. These aspects will be discussed further in Chapter 6.

A very significant feature of a two parameter model is that the coefficient of variation (standard deviation divided by the mean) is dependent only upon the parameter m (or α). Thus for *any* tensile test of *any* sample size, the coefficient of variation is constant if the material is well represented by a two parameter model. The relationship between the coefficient of variation and the parameter m for a two parameter model is illustrated in Figure 4-1.

When sufficient data are available in the literature, the Author has evaluated the parameter m (assuming a two parameter model) using the conventional Class I method previously described and also by comparing mean apparent tensile strengths at different specimen volumes (Class II method). The results are shown in Table 4-1. The m values determined from the Class I method are consistently greater in magnitude than the value of m determined from the Class II method. A potential explanation for this discrepancy is presented later in this chapter.

TABLE 4-1

Weibull Moduli from
Class I and Class II Methods

Rock Type	Test Type	Weibull Modulus		Reference
		Class I	ClassII	
Stripa Granite	Disk Bending	13-14.9	7.8	Swan (1980a)
Stripa Granite	Beam Bending	20.7-23	9.1	Swan (1980a)
St. Cloud Gray Granodiorite	Point Loading	15.3	4.8	Sundae (1974)
Lithonia Granite	Point Loading	9.3	6.5	Sundae (1974)
Rockville Granite	Point Loading	12.2	4.3	Sundae (1974)
Tennessee Sandstone	Point Loading	10.8	8.3	Handin (1969)
Granite	Brazilian	11.4	6.0	Lundborg (1967)

Note: The Tennessee Sandstone data used were those quoted by Sundae (1974) and attributed to Handin (1969).

4.2 THREE PARAMETER MODELS

The Author is unaware of any method for evaluating three parameter model properties that approaches the simplicity of the two parameter methods. The exception to this statement is the approximate methods presented by Weibull (1939a). In a theoretical sense, the σ_u or G_u parameter can be obtained by testing larger and larger specimens in hopes of obtaining an asymptote. However, it is difficult (if not impossible) to establish *a priori* how large a sample is necessary.

The use of the coefficient of variation is also difficult with a three parameter model since it can be easily shown that the coefficient of variation depends upon α, G_u, G_o, V (or S) and the stress distribution in the specimen.

Due to the difficulty in evaluating accurately the frequency histogram, parameters for a three parameter model should be obtained by comparing mean apparent tensile strengths for different tests. In this regard, we may formulate the problem of finding the parameters in the sense of minimizing

$$S = \sum_{i=1}^{N} w_i \left(\bar{T}_i - \bar{T}_a \right)^2 \tag{4-7}$$

where:

w_i	=	weighting factor
N	=	number of distinct test series
$\bar{T}_i$	=	mean apparent tensile strength for test i
$\bar{T}_a$	=	calculated mean apparent tensile strength from Equation (3-3).

Note that $N < 3$ results in an underdetermined system and $N > 3$ results in an overdetermined system. When $N = 3$, the parameters G_u, G_o, and α may be determined such that $S = 0$.

Equation (4-7) is a system of N nonlinear equations in three unknowns. Various methods of solution are available (Beightler *et al* (1979), Dahlquist and Björck (1974)). However, the Author found the damped Gauss-Newton to be far superior to all others.

The minimization of S in Equation (4-7) is accomplished by obtaining the appropriate values of G_u, G_o, and α in the expression for $\bar{T}_a$. The damped Gauss-Newton method is an iterative method which continually *updates* estimations for G_u, G_o and α from some initial *guesses* while continually reducing the magnitude of S. Formally, the method consists of repeatedly solving:

$$\sum_{k=1}^{N} w_k \left(\frac{\partial \phi_k}{\partial x_i}\right)\left(\frac{\partial \phi_k}{\partial x_j}\right) \delta x_i = -\lambda \sum_{k=1}^{N} w_k \left(\frac{\partial \phi_k}{\partial x_i}\right) \phi_k \quad i,j = 1,2,3 \tag{4-8}$$

where:

$$\begin{aligned} \phi_k &= \bar{T}_k - \bar{T}_a \\ x_i &= \text{parameters } (G_u, G_o, \alpha) \\ \delta x_i &= \text{change in } x_i \\ \lambda &= \text{damping factor.} \end{aligned}$$

The parameter values x_i are updated at each solution of Equation (4-8) based upon the increments δx_i until S is zero or nearly so. Qualitatively, the coefficient matrix dictates the direction in the solution space to minimize S and the constants vector dictates the magnitude of displacement in the solution space through which one should transgress.

For highly nonlinear functions ϕ_k, the quasi-linearization assumed in the formulation of the Gauss-Newton method is only appropriate within a small distance from the present solution vector x_i. Thus, the value of λ must be selected to *shorten* the path at each solution of Equation (4-8). In applying the damped Gauss-Newton method in this research, values of λ as low as 10^{-4} were not uncommon. The magnitude of λ must always be sufficiently low so as to ensure monotonic reduction in the magnitude of S.

The function $\bar{T}_a$ typically involves complicated functional forms which invariably contain multiple integrals. The integrals are essentially never expressable in a closed form when $G_u \neq 0$. Thus, the integrals in $\bar{T}_a$ must be evaluated with numerical quadrature (*e.g.*, Ralston (1965)).

The numerical quadrature method selected for solution of problems of this sort must minimize computer roundoff errors. In this regard, the Gauss-Chebychev is a logical choice (Ralston (1965)). Additionally, various orders of numerical integration must be employed so as to assure convergence to the proper solution. In this research, integration orders from 8 to 200 were used. The specific order required depends upon the particular tension test being evaluated as well as the specific integral in the expression for $\bar{T}_a$.

4.3 SIMULATION OF A THREE PARAMETER MATERIAL

One obvious explanation for the discrepancy in the m parameter values obtained for the Class I and Class II methods is that either the local or global failure criterion are inappropriate. While this is perhaps the most palatable explanation, we are left without any means for explaining size effects. A potential explanation of the discrepancy will be presented in this section which does not expand the statistical fracture mechanics models beyond what has been presented thus far.

Recall that the weakest link model leads to an equation for the cumulative probability of failure, G, in terms of the apparent tensile strength, model parameters and the geometric properties of the stress field. In certain situations, this equation can be rearranged so that we may express the apparent tensile strength, T_a, in terms of G, the model parameters and the geometric properties of the stress field. In this form, we may use an unbiased random number generator to generate values of G between 0 and 1 and thus, calculate *experimental* values of T_a for assumed model parameters (Robinson (1970)). In this manner, we may dictate the material behavior and observe the test data that would be representative of the material.

The test which will be simulated in the above manner is for homogeneous uniaxial tension. We shall assume the defects to be either volumetrically or surfacially distributed (one or the other; not both). We shall use the *incomplete* form of the risk of rupture for a two or three parameter model. In other words, only defects whose normals are coincident with the principal stress axis will be considered to contribute to the risk of rupture. The incomplete form is used since it allows a closed form statement of $T_a = f(G)$ whereas the *complete* form does not. It will be obvious later that the complete form would lead us to the same conclusions that we will obtain in this section with the incomplete form. We will take the volume or surface area and the scaling parameter σ_o (G_o) to be unity. Further, the value of σ_u will be expressed as some proportion, λ, times the modal value of the apparent tensile strength. Once a set of N experiments has been generated on the computer for a specific two or three parameter model, we will evaluate the m parameter assuming a two parameter model. The Class I method discussed in Section 4.1 is used.

The results of a series of the above simulations is presented in Figure 4-2 in terms of the ratio of m determined by the least squares method, m_{ls}, to the input value of m as a function of the number of experiments. As illustrated in this figure, the ratio becomes large as the value of σ_u increases. Although the very early portion of each of the curves depends on the specific random number generator, one can reasonably conclude that 70 or more direct tension tests are required to adequately determine the value of m when $\sigma_u = 0$.

One might feel that experimental data from a three parameter model could be identified as such by observing the data in the space of Equation (4-4). However, this is not always the case. The computer generated data for one of the three parameter simulations is shown in the space of Equation (4-4) in Figure (4-3). Concavity (indicative of suggesting a three parameter model) is absent from this figure.

Although a multitude of explanations can be put forth for the discrepancy between Class I and Class II methods of obtaining the values of m, the explanation just given accounts for the inconsistency while still retaining both the local and global failure criterion.

CHAPTER 5

LABORATORY EXPERIMENTS

During the course of this research four different types of tension tests were performed:

(1) Four point bending
(2) Brazilian or split cylinder
(3) Hydraulic fracturing
(4) Rubber fracturing.

The first two tests are commonly employed for rock testing (Goodman, 1980). The third was popularized by Haimson (1968) and the last test was designed by the Author. Each of the tests will be described in this chapter and the associated risk of rupture for $G_u = 0$ will be presented for all except the Brazilian test. Derivations for the risk of rupture for the individual tests for $G_u \neq 0$ are given in Appendix B.

5.1 FOUR POINT BENDING

A special fixture was fabricated for four point bending of three different rock beam cross-sections; circular, square and diamond. Employing Classical Beam Theory, the uniaxial inhomogeneous stress field in the beam is found as;

$$\sigma = \begin{cases} \dfrac{PLy}{6I} & 0 \leqslant x \leqslant \dfrac{L}{6} \\ \dfrac{PLy}{4I}\left(1 - \dfrac{2x}{L}\right) & \dfrac{L}{6} \leqslant x \leqslant \dfrac{L}{2} \end{cases} \tag{5-1}$$

where:

P = applied load

L = beam length

I = moment of inertia.

The coordinate system is defined in Figure 5-1. The apparent tensile strength is defined as;

$$T_a = \frac{PLa}{12I} \tag{5-2}$$

Therefore, the stress at rupture can be stated as;

$$\sigma = \begin{cases} \dfrac{2\,T_a y}{a} & 0 \leqslant x \leqslant \dfrac{L}{6} \\ \dfrac{3\,T_a y}{a}\left(1 - \dfrac{2x}{L}\right) & \dfrac{L}{6} \leqslant x \leqslant \dfrac{L}{2} \end{cases} \tag{5-3}$$

The functional form (linearity in both x and y) is identical for each beam cross-section. The risk of rupture for each beam cross-section assuming volumetric flaws is as follows.

CIRCULAR

$$B = \frac{V}{12\pi\alpha}\left[\frac{T_a{}^2}{G_o}\right]^{\alpha}\left[\frac{2\alpha+3}{2\alpha+1}\right]\frac{\Gamma(\alpha+\frac{1}{2})\Gamma(\frac{3}{2})}{\Gamma(\alpha+2)} \tag{5-4}$$

where:

Γ = the gamma function.

SQUARE

$$B = \frac{V}{24\alpha}\left[\frac{T_a{}^2}{G_o}\right]^{\alpha}\left[\frac{2\alpha+3}{(2\alpha+1)^2}\right] \tag{5-5}$$

DIAMOND

$$B = \frac{V}{24\alpha}\left[\frac{T_a{}^2}{G_o}\right]^{\alpha}\left[\frac{1}{\alpha+1}\right]\left[\frac{2\alpha+3}{(2\alpha+1)^2}\right] \tag{5-6}$$

Under the assumption of surface flaws, the associated two parameter risks of rupture are as follows.

CIRCULAR

$$B = \frac{aL}{24\alpha}\left[\frac{T_a^{\,2}}{G_o}\right]^{\alpha}\left[\frac{2\alpha+3}{2\alpha+1}\right]\frac{\Gamma(\alpha+\frac{1}{2})\Gamma(\frac{1}{2})}{\Gamma(\alpha+1)} \tag{5-7}$$

SQUARE

$$B = \frac{aL}{6\alpha}\left[\frac{T_a^{\,2}}{G_o}\right]^{\alpha}\left[\frac{(\alpha+1)(2\alpha+3)}{(2\alpha+1)^2}\right] \tag{5-8}$$

DIAMOND[1]

$$B = \frac{aL}{24\alpha}\left[\frac{T_a^{\,2}}{G_o}\right]^{\alpha}\left[\frac{2\alpha+3}{(2\alpha+1)^2}\right] \tag{5-9}$$

By equating risks of rupture, the ratios of the apparent tensile strengths (at constant G) can be found between any two tests assuming either surface or volume flaws. The ratio of the strengths between the diamond and the square cross-sections is given in Figure 5-2 as a function of m (α). Figure 5-3 illustrates the ratio of the strength of the circular cross-section to the square cross-section. If the material being tested was well characterized by a two parameter model, the parameter, α, could be evaluated from either of these two figures. It is easily shown that similar figures can not be constructed for a three parameter model since the ratio of the strengths would depend upon the volume (or surface area) of the beams being tested. In fact, as the size of the beams increases, the ratio of the apparent tensile strength of any cross-section to that of another cross-section would tend to unity.

Vardar (1975) has stated that the friction at the supports of bending fixtures should be evaluated and taken into account. The observed apparent tensile strength will be greater than that experienced by the rock if a non-zero coefficient of friction is present. In this regard the observed apparent tensile strengths must be reduced by the factor;

[1]In all equations for the risk of rupture for diamond beams, the quantity a is the beam width; however, in Equations (5-2) and (5-3), a is the corner-to-corner dimension.

$$1 - 3\frac{\mu(P)\,a}{L} \tag{5-10}$$

Vardar (1975) and Swan (1980a), (1980b) considered $\mu(P)$ to be constant. This was not found to be the case in the Author's laboratory work. The experimental function $\mu(P)$ is shown in Figure 5-4. It is of interest to note that if $\mu(P)$ is not constant, the load/deformation curve will be nonlinear even if the material being tested is linear. Thus, testing methods which rely on changes in compliance in bending with differences in applied loading (*e.g.* Hardy *et al* (1973), Swan (1980a), (1980b)) may provide erroneous conclusions if the appropriate data reduction is not performed.

Vardar (1975) discusses the fact that one may determine whether volumetrically or surfacially distributed defects are responsible for rupture by bending rectangular beams in two different manners. First, the beams are tested in such a way that the neutral axis is coplanar with the largest cross-section dimension. In the second case, the testing is done with the neutral axis coplanar with the smallest cross-sectional dimension. If the mean strengths from both testing methods agree, then a two parameter model with volumetrically distributed flaws is indicated. Otherwise, a surface flaw model may be suggested as a possible mechanism. Vardar (1975) found that in one case surface flaws were suggested and in another volumetrically distibuted flaws were indicated. The rock type used by Vardar in this testing was Sierra White Granite. Testing in this research indicated that this rock does not satisfy the material behavior assumptions neccessary for the application of currently used statistical fracture mechanics models. Further discussion of Sierra White Granite is given in Chapter 6.

5.2 BRAZILIAN TEST

The Brazilian or split cylinder test (Carniero and Barcellos (1953)) is used extensively in the rock mechanics community. In this test, *thin* sections (see Wijk (1978) for a definition of *thin*) of core are diametrically loaded until rupture occurs splitting the disc along a surface coplanar with the applied load (see Figure 5-5). Often, the loading surfaces

are milled slightly to decrease the local crushing resulting from point loading.

The risk of rupture for a two parameter Weibull model assuming volumetrically distributed flaws is given elsewhere (Vardar (1975), Vardar and Finnie (1975)) and will not be repeated here. This test was not extensively used in this research and the derivation for the risk of rupture for the three parameter model is not given.

5.3 HYDRAULIC FRACTURING TEST

The testing configuration used for hydraulic fracturing experiments is similar to that employed by Haimson (1968). As shown in Figure 5-6, a central hole is drilled concentrically part way through a circular core. A stainless steel pipe is epoxied in the upper portion of the drillhole and mates to a special loading platen which also contains the flow path for the fracturing fluid (in this case, tapwater). A small axial load is applied to ensure that the fracture will be vertical. This small applied vertical load is neglected in the calculation of the risk of rupture. Neglecting end effects, the stress distribution for this test configuration is available in most introductory solid mechanics texts (*e.g.* Timoshenko and Goodier, 1970). Under the assumptions of surface flaws the risk of rupture for a two parameter model can be shown to be

$$B = \frac{A_h}{2\pi}\left[\frac{T_a^{\,2}}{G_o}\right]^{\alpha}\int_{-\frac{\pi}{2}}^{\frac{\pi}{2}}\int_{-\frac{\pi}{2}}^{\frac{\pi}{2}} F^{2\alpha}\cos(\phi)\; d\phi\; d\psi \tag{5-11}$$

where:

A_h = surface area of internal borehole

$F = \cos^2(\phi)\cos^2(\psi) + \gamma\sin^2(\psi)$

$$\gamma = \left[\frac{1-\left(\frac{b}{a}\right)^2}{1+\left(\frac{b}{a}\right)^2}\right]$$

a = internal borehole radius

b = core radius.

Note that contributions from the top and bottom surfaces have been neglected.

The two parameter risk of rupture assuming volumetrically distributed flaws is;

$$B = \frac{V_h}{\pi}\left[\frac{T_a^{\,2}}{G_o}\right]^{\alpha}\int_{1}^{\frac{b}{a}}\int_{-\frac{\pi}{2}}^{\frac{\pi}{2}}\int_{-\frac{\pi}{2}}^{\frac{\pi}{2}} F^{2\alpha}\cos(\phi)\; d\phi\; d\psi\; \rho\; d\rho \qquad (5\text{-}12)$$

where:

V_h = volume of internal borehole

$$F = \gamma_1\cos^2(\phi)\cos^2(\psi) + \gamma_2\sin^2(\psi)$$

$$\gamma_1 = \left[\frac{1+\left(\frac{b}{\rho a}\right)^2}{1+\left(\frac{b}{a}\right)^2}\right]$$

$$\gamma_2 = \left[\frac{1-\left(\frac{b}{\rho a}\right)^2}{1+\left(\frac{b}{a}\right)^2}\right]$$

The function F in Equations (5-11) and (5-12) is only defined in the positive domain. Thus, with the integration limits given in these equations, negative values of F are discarded (see Appendix B). In both of the preceeding forms of the risk of rupture, the rock has been assumed to be impermeable to the fracturing fluid. If the fracturing fluid acts on the defect faces, the mean apparent tensile strength in Equation (3-3) (with the risk of rupture from Equation (5-11)) is merely reduced by a factor of two. The risk of rupture for volumetrically distributed flaws in porous materials is exceedingly more complex than for impermeable materials.

5.4 RUBBER FRACTURING TEST

The rubber fracturing test (see Figure 5-7) is similar to the hydraulic fracturing experiment. However, in this test the rock specimen is significantly smaller in the axial dimension and the loading is provided by rubber rather than a fluid. Six specific test geometeries are employed as shown in Table 5-1. The rubber cylinders in this test are cut from *cording stock* fabricated of synthetic rubber commercially known as Buna-N. The nominal bulk modulus is approximately 200-300 MPa (*Handbook of Molded and Extruded Rubber* (1949)).

The stress distribution in the rock specimen in this test is the superposition of the two separate loadings at the borehole surface;

(1) constant radial pressure
(2) axially varying shear.

The first loading is dependent upon the fact that the rubber itself can not sustain shear stresses; thus, $\sigma_z = \sigma_r = \sigma_\theta$ in the rubber cylinder. The stress distribution is obviously the same as in the hydraulic fracturing test.

TABLE 5-1

Rubber Fracturing
Test Configurations

Data Set	O.D. (mm)	I.D. (mm)	t (mm)
A	62	6.4	12.7
B	62	6.4	25.7
C	62	9.5	12.7
D	62	9.5	25.7
E	62	12.7	12.7
F	62	12.7	25.4

Before discussing the solution to the second loading, it is instructive to consider a similar problem given by Goodman (1980). Goodman discusses the stress distribution in a semi-infinite medium which contains a semi-infinite circular cylinder loaded axially. Neglecting radial variations in vertical stress in the circular cylinder and considering frictional contact at the cylindrical surface, Goodman finds the vertical stress in the pile to be;

$$\sigma_y = p\, e^{-\left[\frac{2\nu_c\mu}{(1-\nu_c) + (1+\nu_r)\frac{E_c}{E_r}} \frac{y}{a}\right]} \tag{5-13}$$

where:

subcripts c, r	=	pile and rock,respectively
ν	=	Poisson's ratio
E	=	Young's modulus
a	=	pile radius.

At the surface of the semi-infinite medium, $\sigma_y = p =$ *applied pressure*. Further, the radial stress at the contact is found to be;

$$\sigma_r = \left[\frac{\nu_c}{(1-\nu_c) + \frac{E_c}{E_r}(1+\nu_r)}\right]\sigma_y \tag{5-14}$$

For $\frac{E_c}{E_r}$ small and $\nu_c = ½$, $\sigma_r = \sigma_y$. Thus, we may conclude for the rubber fracturing experiment that the second loading (axially varying shear) does not affect the stress state on the upper and lower surfaces of the rock discs. Although the stresses within the disc are altered by the shear on the borehole wall, we will find in Chapter 6 that this solution is unnecessary; thus, it will not be derived here.

The only risk of rupture for the rubber fracturing which will be given here is for the two parameter model assuming surfacially distributed flaws, *viz*;

$$B = 2a^2 \left[\frac{T_a^{\,2}}{G_o} \right]^{\alpha} \int_1^{\frac{b}{a}} \int_{-\frac{\pi}{2}}^{\frac{\pi}{2}} \int_{-\frac{\pi}{2}}^{\frac{\pi}{2}} F^{2\alpha} \cos(\phi)\, d\phi\, d\psi\, \rho\, d\rho \tag{5-15}$$

The function F is given in Equation (5-12). Note that we have neglected the risk of rupture contributions from the borehole surface (due to the shear). Justification will be given in Chapters 6 and 7.

CHAPTER 6

EXPERIMENTAL RESULTS

In this chapter, the results of the 600 plus tests performed during this research will be presented. Analysis of these results is presented both in this chapter and in more detail in Chapter 7. Except for the hydraulic fracturing experiments, all loadings were accomplished with a 700 KN Riehle loading frame. Loading rates were controlled so as to obtain stress rates of approximately 3-5 MPa/min.

6.1 FOUR POINT BENDING-CARRARA MARBLE

Specimens for rectangular and diamond cross-sections were obtained by sawing beams with long axis along any of the three orthogonal directions in the rectangular parent block. Final finishing of the beams to square cross-section with a width of 2.4 cm was accomplished with a diamond impregnated grinding wheel. Circular cross-section beams were obtained by coring in the three principal directions of the parent block with a thin walled 2.54 cm diameter coring bit.

All of the Carrara Marble beams were tested in a loading fixture with L (see Figure 5-1) equal to 12.7 cm.

The experimentally determined strengths were corrected for friction as discussed in section 5.1. The number of tests in each data set and the experimentally determined mean apparent tensile strengths and associated variances are given in Table 6-1. The data are presented in the functional space given by Equation (4-4) in Figure 6-1 thru Figure 6-3 for each cross-section. The value of m_{ls} for various groups of data is also given in these figures. The value of m_{ls} will also be referred to as the apparent Weibull Modulus, m_a. One significant observation which can be made from the data presented in these figures is

TABLE 6-1

Four Point Bending Results
Carrara Marble

Data Set	N	$\bar{T}_a$ (MPa)	Variance $(MPa)^2$
Square (Set 1)	28	17.7	0.97
Square (Set 2)	3	11.1	-
Circular (Set 1)	15	17.6	1.06
Circular (Set 2)	17	13.5	0.49
Circular (Set 3)	27	18.6	1.75
Diamond (Set 1)	6	20.7	0.12
Diamond (Set 2)	6	15.9	1.13
Diamond (Set 3)	19	25.3	2.35

that the Carrara Marble is anisotropic with respect to the apparent tensile strength. Although the Carrara Marble may well process a *simplified anisotropy* (e.g., orthotropic), one can not establish this without further testing in other directions.

Another observation can be made concerning the Carrara Marble results which is perhaps more significant than the apparent strength anisotropy. Specifically, the size effect (as qualitatively indicated by the value of m_a) is diferent in each direction. Thus, not only is the Carrara Marble anisotropic, but the *degree of anisotropy* is dependent upon the specimen size. Conceivably, there exists sample sizes with which anisotropy would not be

detectable.

Volkov (1962) states that Bartenev and Bovkunenko (1956) were the first to detect anisotropy of size effect in glass filaments. Although this experimental observation may be common in the ceramics literature, the Author is unaware of any publication where the anisotropy of size effect in rock is discussed.

If we for the moment assume that failure inducing defects are either mineral or crystal interfaces (or differential mineral locations) it becomes physically obvious that there should be an anisotropy of size effect since all rocks contain elongated minerals of some sort.

Weibull (1939b) presents a theory for anisotropic materials. However, the assumptions necessary for the application are significant and can not be tested for the Carrara Marble with the limited data obtained in this research. Therefore, we will only note here that the ratio of strengths for different cross-sections are significantly higher than those which would be predicted using m_{ls} and the Class II method given in Figures 5-2 or 5-3.

6.2 FOUR POINT BENDING-SIERRA WHITE GRANITE

Beams of Sierra White Granite were prepared following the same proceedures as were described for the Carrara Marble. The final width of the square shaped beams was 1.9 cm. The bending fixture used for the Sierra White Granite had L = 7.6 cm. The diameter of the circular beams was 1.9 cm.

Square and diamond shaped cross-sectional beams were tested from only one principal axis of the parent block, However, circular beams were tested in each of the three principal directions in an effort to evaluate any anisotropy.

The number of tests in each data set and the experimentally determined mean apparent tensile strengths and associated variances are given in Table 6-2. The experimentally determined strengths (corrected for friction) are shown in Figures 6-4 thru 6-6 for

TABLE 6-2

Four Point Bending Results
Sierra White Granite

Data Set	N	$\bar{T}_a$ (MPa)	Variance $(MPa)^2$
Square (Set 3)	15	19.7	8.37
Circular (Set 1)	15	13.7	0.41
Circular (Set 2)	16	15.0	4.16
Circular (Set 3)	16	19.7	4.85
Diamond (Set 3)	15	23.2	4.72

each cross-section using the space defined by Equation (4-4). Two features of these figures are worthy of comment. Firstly, the concavity illustated in several of the three figures indicates the inappropriateness of a two parameter model. Secondly, as was the case with the Carrara Marble, the Sierra White Granite displays strength anisotropy as well as anisotropy of size effect. One may reasonably conclude that the results indicate that the Sierra White Granite is transversly isotropic with respect to mean apparent tensile strength. Data sets 1 and 2 for circular cross-section beams appear to be indistinguishable within the usual experimental error. However, the results from data set 3 are distinct from the other two sets.

Skilled labor forces in granite quarries have long recognized the orthotropic strength features through the use of the terms *strong way* and *weak way*. Since the parent block used to obtain the Sierra White Granite beams was obtained from quarrying operations, we may reasonably conclude that the free surfaces of the parent block are coincident with prin-

cipal strength planes. Thus, if the rock were transversly isotropic *in situ* we would expect to note a transverse isotropy from the laboratory testing program and *vice versa.*

As was the case with the Carrara Marble, the anisotropy of the Sierra White Granite negates the use of the statistical fracture mechanics models presented in this Thesis. However, we again note that the value of m_a in concert with the Class II method of Figure 5-2 or 5-3 indicates that the ratio of the mean diamond strength to the mean square strength and the mean circular strength to the mean square strength should be lower than those observed.

Vardar (1975) used Sierra White Granite (among other rock types) for investigating statistical fracture mechanics models. Due to the anisotropy observed in the present testing, it is difficult to assess Vardar's results since he does not give any information relative to the orientation of test specimens with respect to the parent block.

6.3 FOUR POINT BENDING-STRIPA GRANITE

Beams of Stripa Granite were prepared following the same proceedures as were described fo the Carrara Marble. The final width of the square shaped beams was 1.9 cm. The bending fixture used for the Stripa Granite had L = 7.6 cm. The diameter of the circular beams was 1.9 cm.

The mean apparent tensile strength for each of the cross sections is given in Chapter 7. The experimentally determined strengths (corrected for friction) are illustrated in Figures 6-7 thru 6-9 for each cross-section using the space defined by Equation (4-4). The anisotropy illustrated by the Carrara Marble and the Sierra White Granite is not apparent in the Stripa Granite results.

6.4 RUBBER FRACTURING-STRIPA GRANITE

As noted in Table 5-1, six distinct specimen sizes were used in the rubber fracture testing of Stripa Granite. For each central borehole diameter, the height of the specimen was varied so as to evaluate whether volumetric or surfacial flaws were responsible for fracture. Top and bottom surfaces were diamond saw cuts and the central holes were drilled with diamond impregnated core bits.

Swan (1980b) has stated that size effects in fracture of Stripa Granite are due to subcritical crack growth and the subsequent relationship of the apparent crack length at rupture to the dimensions of the specimen. Swan used changes in compliance in addition to linear elastic fracture mechanics to arrive at this conclusion. In order to evaluate subcritical crack growth, many of the rubber fracturing specimens were instrumented to monitor acoustic emissions. A Dunegan/Endevco 3000 series acoustic emission system was used to monitor the subaudible noise in the rubber fracturing tests. The transducer used was a S9204 with a frequency response of approximately 100-300 KHz. The preamplifier was a model 1801-190B.

Without exception, acoustic emissions were not detected by the experimental apparatus until rupture occurred indicating negligible subcritical crack growth.

Subcritical crack growth *can* occur in many rocks and rock-like materials. For example, the load and associated acoustic emission as a function of loading time for a rubber fracturing test of concrete is shown in Figure 6-10. The inner and outer diameters of the specimen are 1.3 and 7.6 cm and the borehole height is 1.3 cm. As can be observed in this figure, significant acoustic emission (indicative of subcritical crack growth or "microcracking") initiates at about 40% of the ultimate load.

The mean apparent tensile strength and number of individual tests for each of the rubber fracturing test series is given in Table 6-3. The apparent tensile strengths given in this table are significantly higher than those typically reported for granites and might well be

TABLE 6-3

Rubber Fracturing Test Results

Data Set	$\bar{T}_a$ (MPa)	Number of Tests
A	72.3	42
B	73.5	34
C	49.0	67
D	48.0	47
E	39.1	31
F	39.2	17

discarded by many practicing engineers. However, reported values of *tensile strength* typically are obtained from Modulus of Rupture or Brazilian testing which usually involves significantly greater specimen volumes or surface areas. The other notable observation which can be drawn from Table 6-3 is that the mean apparent tensile strength is *independent* of the specimen height (within experimental error bounds). Thus, we may readily conclude that the apparent tensile strength in this test is *independent* of specimen volume. Further, since the mean apparent tensile strength does not depend on specimen height, we may conclude that the contribution to the risk of rupture from the borehole surface is negligible. Thus, the shear at the rubber/rock interface (see Chapter 5) renders a negligible value of the risk of rupture at the borehole wall. Therefore, the data sets may be categorized as to internal borehole size. In this regard, the apparent tensile strengths for each of the three borehole sizes is shown in the space dictated by Equation (4-4) in Figures 6-11 thru 6-13. The linear least squares fit for each case is also illustrated in these figures. The concavity indicative of the inadequacy of a two parameter model is much more apparent for the Stripa

Granite than the other rock types discussed previously.

Stripa Granite is profuse with *healed* (mineralized) fractures. Although attempts were made to prepare only specimens which did not contain healed fractures, a significant number were prepared which contained fractures intersecting the internal borehole. The apparent tensile strengths from these specimens are not directly useful to this research; however, it is interesting to note that the mean strength for specimens with a single randomly oriented fracture is of the order of 60% of that for the intact specimens.

The apparent deformation modulus can be calculated for the rock discs by noting the slope of the load/deformation curve, the disc dimensions and the bulk modulus of the rubber. This calculation was performed for all rubber fracturing tests. The mean apparent deformation modulus of the intact rock discs is found to be approximately twice the mean of some 50 discs with single, randomly oriented healed fractures intersecting the internal borehole.

6.5 HYDRAULIC FRACTURING-STRIPA GRANITE

Hydraulic fracturing of Stripa Granite cores was accomplished by pressurizing the internal borehole (see Figure 5-4) at a rate of approximately 7 Mpa/min. A constant flow rate pump was used to apply the internal borehole pressure. Two different internal borehole diameters were used; specifically, 0.7 cm (set 1) and 1.3 cm (set 2). Twenty two tests were performed in set 1 and twenty three tests were performed in set 2. The mean apparent tensile strengths were found to be 16.2 MPa and 12.8 MPa, respectively. The nominal axial load applied during the hydraulic fracturing tests was 5 Mpa.

Acoustic emission was monitored in all of the hydraulic fracturing tests. No activity was detected prior to rupture except in cases where slight system leaks (usually at the stainless steel tube/loading fixture interface) occurred. Zoback *et al* (1977) reported acoustic emission activity prior to rupture. However, these investigators were testing a sandstone which could be expected to be emitting subaudible noise from subcritical crack growth as

well as from fluid flow in the rock matrix.

6.6 BRAZILIAN TESTING-STRIPA GRANITE

Brazilian tests of Stripa Granite were performed to provide a quantiative comparision between the Stripa Granite tested in this research to the Stripa Granite tested by Swan (1980a), (1980b). Efforts were made to obtain geometric similarity with Swan's tests; however, Swan's specimens were fabricated from slightly larger core.

The results for the Brazilian tests from this research as well as those of Swan are given in Table 6-4. The mean apparent tensile strength is lower for the rock used in this research; however, it is difficult to make any definitive comparison with so few tests.

TABLE 6-4

Brazilian Test Results

Data Set	t (mm)	a (mm)	2α (o)	N	$\bar{T}_a$ (MPa)
Swan (1980a)	18.2	35.8	22	24	18.9
Present Work	15.8	30.6	22	23	15.5

CHAPTER 7

ANALYSIS OF EXPERIMENTAL RESULTS

In this chapter, the Stripa Granite parameters will be evaluated for the three parameter model with strain energy release rate as the variant. The rubber fracturing tests are used to obtain the value of the parameters since the greatest number of tests were of this type. After evaluating the model parameters the model is used to estimate the mean apparent tensile strengths in the bending and hydraulic fracture experiments performed in this research. The model will also be used to estimate the mean apparent tensile strength for a series of tests reported by Swan (1980a). Finally, the model will be used to estimate the *in situ* apparent tensile strength in a field hydraulic fracturing test in Stripa Granite reported by Doe *et al* (1981).

7.1 DETERMINATION OF PARAMETERS

In order to evaluate the parameters of the three parameter model, the damped Gauss-Newton method described in Chapter 4 is used. The values of the weighting functions w_i are calculated as the ratio of the number of tests at diameter i to the total number of rubber fracturing tests performed.

As observed in Chapter 6, contributions to the risk of rupture are only significant on the upper and lower surfaces of the discs. Therefore, we shall substitute Equation (5-15) for B into Equation (3-3) for the mean apparent tensile strength, $\overline{T}_a$.

The Gauss-Newton minimization results in values of the parameters as follows;

$$G_u^{1/2} = 10.5 \text{ MPa}$$

$$G_o = 0.159\ (10^{-4})\ MPa^2 - m^{\frac{2}{\alpha}}$$

$$\alpha = 0.525$$

The value of α determined is significantly lower than any value of $\alpha = \frac{m}{2}$ determined by the Class I method discussed in Chapter 4. The values of the parameters imply qualitatively that the risk of rupture is nearly proportional to the square root of the strain energy release rate above and beyond a certain threshold value.

7.2 FOUR POINT BENDING TESTS

Since we have experimentally established that rupture of Stripa Granite is due to surfacially distributed flaws, the model implyed in section 7.1 will be used in the approriate risks of rupture for each beam cross-section tested in four point bending. The forms of the risk of rupture for these cases is given in Appendix B. Using the parameter values of section 7.1, the mean apparent tensile strengths are given in Table 7-1.

Swan (1980a) reports mean apparent tensile strengths for circular Stripa Granite beams tested in four point bending. Set A has a diameter of 2.10 cm and a length of 5.0 cm. Set B has a diameter of 4.16 cm and a length of 10.0 cm. Set C has a diameter of 5.20

TABLE 7-1

Estimated and Experimental Bending Results

Cross Section	Experimental $\bar{T}_a$ (MPa)	Estimated $\bar{T}_a$ (MPa)	Error (%)
Square	21.1	20.3	4
Circular	25.3	24.0	5
Diamond	28.0	27.5	2

cm and a length of 12.1 cm. The results of the estimated mean apparent tensile strengths are are given in Table 7-2.

The estimated mean apparent tensile strengths are not as accurate as was the case in the four point bending performed in this research. At least two reasons exist for the error in estimation, *viz*;

(1) Swan's results are not corrected for friction.

(2) The Stripa Granite used by Swan was not extracted from the same location as the rock used in this research.

7.3 LABORATORY HYDRAULIC FRACTURING TESTS

The estimated mean apparent tensile strengths assuming surfacially distributed flaws and the three parameter model of section 7.1 are 15.0 MPa and 13.8 MPa for the 0.7 cm and 1.3 cm internal diameter boreholes, respectively. The estimated magnitudes differ from the experimentally determined values by 7% and 8%, respectively.

TABLE 7-2

Estimated and Experimental Bending Results
(After Swan (1980a))

Data Set	Experimental $\bar{T}_a$ (MPa)	Estimated $\bar{T}_a$ (MPa)	Error (%)
A	27.6	28.9	5
B	24.2	18.2	25
C	19.7	16.5	16

The Author had the preconceived notion that calculation of the mean apparent tensile strength for a hydraulic fracture experiment would necessitate the inclusion of fluid pressure on the defect faces. The above calculations did not include this pressure. The exclusion of the pressure on the defect faces resulting in the excellent agreement between estimated and experimental results indicates that the failure inducing defects may well be *soft* minerals imbedded in a *stiffer* matrix material rather than actual voids.

7.4 DISK BENDING

Swan (1980a) reports results of disk bending tests (see Figure 7-1) on three different disc sizes of Stripa Granite. In analyzing the results, Swan assumed that the discs were simply supported at the outer periphery. This assumption is consistent with Gorham and Rickerby (1975) whom Swan referenced.

Swan strain gauged the lower (free) surface of a disc and monitored the radial and tangential strain as a function of the applied loading. The radial strain exhibited a distinct concavity while the tangential strain did not.

Whereas Swan attributed the concavity in the load/radial strain curve to microcracking or subcritical crack growth, the Author feels the concavity was due to a changing support condition at the disc periphery. In other words, as the load is increased, the support goes from a simple support condition to a nearly *clamped* condition. This situation would result in nonlinear radial strain without a significant change in linearity for the tangential strain. Qualitatively, this load/stain behavior was reported by Swan. The dimensions of the discs tested by Swan are given in Table 7-3.

The stress distribution for this bending test is presented by Timoshenko and Lessels (1925) for both simple and clamped supports. Using these distributions, the mean apparent tensile strengths are calculated using the three parameter model of section 7.1 with the assumption of surfacially distributed flaws. The experimental results of Swan and the estimated mean apparent tensile strengths are given in Table 7-4.

TABLE 7-3

Dimensions of Discs Tested in Bending
(After Swan (1980a))

Data Set	a_1 (mm)	t (mm)
B	21.8	5.3
C	24.5	6.0
D	47.5	11.6

TABLE 7-4

Estimated and Experimental Disc Bending Results

Data Set	Experimental $\bar{T}_a$ (*MPa*)	Estimated $\bar{T}_a$ (MPa)	
		Simple Support	Clamped Support
B	35.5	16.7	42.7
C	31.1	15.8	39.6
D	25.4	12.8	28.6

7.5 FIELD HYDRAULIC FRACTURING TESTS

As mentioned in Appendix A, the Stripa Granite for this testing program was obtained from the SBH-4 borehole near the Stripa Mine, Sweden. A series of field hydraulic fracturing tests were performed in this drillhole and the results of those tests are reported by Doe *et al* (1981).

The apparent tensile strength in an *in situ* hydraulic fracturing experiment depends on the *in situ* stress state since the calculation of the risk of rupture involves the region of ten-

sile stress defined by the components of the stress tensor. However, the estimate of the apparent tensile strength performed in this research will neglect the *in situ* stress. The justification is taken from the experimental results presented by Haimson (1968) which indicate that confining pressure applied to the periphery of laboratory hydraulic fracture test specimens does not significantly alter the apparent tensile strength for granites and quartzites.

Using the model parameters of section 7.1, the *packed off* dimensions given by Doe *et al* (1981) and neglecting end effects, the mean apparent tensile strength for the *in situ* tests is estimated as 10.7 MPa. This value of mean apparent tensile strength is essentially equal to the value of the parameter $G_u^{1/h}$ due to the relatively large surface area in the field test borehole.

7.6 STATISTICAL MOMENTS

As was discussed in Chapter 4, parameters for two parameter models may be evaluated from the frequency histogram (or cumulative distribution function) for a single test or by comparing statistical moments from different test series. When a frequency histogran method is used, the resulting model usually accurately reproduces the experimental frequency distributions but may be inaccurate when applied to tests of different specimen size or type.

In this Thesis, parameters of the statistical fracture mechanics model are obtained by considering the mean apparent tensile strength from different size tests. If the resulting model is an accurate characterization of the material, we would expect that the model could accurately estimate the frequency histogram for a given test series.

The three parameter model determined for the Stripa Granite does not accurately estimate the characteristics of the experimental frequency histogram with the exception of the mean value. The estimates and experimentally determined statistical moments for the rubber fracturing tests are given in Table 7-5. The second and third moments are with

respect to the mean.

The descrepancy between the estimated and experimentally determined statistical moments may be attributed to several factors. Firstly, accurate statistical moments are very difficult to determine experimentally. A significantly greater number of tests may be required than were performed in this research. The first and second moments illustrate a decreasing magnitude with respect to an increase in borehole diameter. However, the third moment displays a sign change as the internal borehole diameter increases suggesting that the experimentally determined moment is inaccurate, to say the least. Secondly, the local criterion considering only Mode I fracture may not result in an accurate characterization of the Stripa Granite. This is an aspect of statistical fracture mechanics which requires more extensive research.

Table 7-5

Estimated and Experimental Statistical Moments of Rubber Fracturing Tests

Data Set	Experimental Moment (Estimated Moment)		
	First (MPa)	Second $(MPa)^2$	Third $(MPa)^3$
A + B	72.8 (74.5)	53.0 (1750.)	-10600. (-11200.)
C + D	48.6 (50.0)	16.8 (550.)	1670. (-5040.)
E + F	39.1 (39.0)	13.7 (270.)	-400. (-3110.)

CHAPTER 8

CONCLUSIONS AND RECOMMENDATIONS

Several significant conclusions may be drawn from the experimental results and analysis presented in this Thesis. Firstly, the two parameter models previously used in the literature to analyze the size effect in rock may be inappropriate for many brittle rock types. The three parameter model with strain energy release rate as the statistical variant was found to be appropriate for characterizing the mean apparent tensile strengths for different types of tests of Stripa Granite. Secondly, surfacially distributed flaws rather than volumetrically distributed flaws are responsible for rupture in many testing situations. Thirdly, anisotropy (both in apparent tensile strength and size effect) precludes the use of contemporary statistical fracture mechanics models for many brittle rocks.

Subordinate conclusions can be drawn from this research as well as from examining the results of others in the literature. Load dependent friction should always be evaluated and taken into account when analyzing bending tests. The degree of anisotropy should always be evaluated prior to attempting to apply contemporary statistical fracture mechanics models.

Recommendations for further research can also be readily formulated from the results presented in this Thesis. Fundamental research into size effects in compression would benefit the practicing engineer greatly. This research would involve substantive efforts into the character of the failure inducing defects as well as the local failure criterion. Additionally, development of statistical fracture mechanics models for anisotropic rock would broaden the spectrum of rock types which could be analyzed with statistical fracture mechanics.

REFERENCES

Baecher, G.,"The size effect in brittle fracture", Master of Science Thesis, Massachusetts Institute of Technology (1970).

Bartenev, G.M. and Bovkunenko, A.N., "Strength of glass fibers and the effect of various factors upon their strength", *ZhTF, 26,* No. 11, 2058 (1956).

Beightler, C.S., Phillips, D.T. and Wilde, D.J., *Foundations of Optimization,* Prentice Hall (1979).

Benjamin, J.R. and Cornell, C.A., *Probability, Statistics and Decision for Civil Engineers,* McGraw-Hill (1970).

Brace, W.A., "Brittle fracture of rocks", In *State of Stress in the Earth's Crust,* W.R. Judd, editor, pp111-180 (1964).

Carniero, F.L.L.B. and Barcellos, A., *Union of Testing and Research Laboratories for Materials and Structures,* No. 13 (1953).

Cornet, I. and Grassi, R.C., "Fracture of inoculated iron under biaxial stresses", *Journal of Applied Mechanics, 54,* pp172-174 (1955).

Doe, T., Ingevald, K., Strindell, L., Haimson, B.C. and Carlsson, H., "Hydraulic fracturing and overcoring stress measurements in a deep borehole at the Stripa test mine, Sweden", 22nd U.S. Symposium on Rock Mechanics, Cambridge (1981).

Dahlquist, G. and Björck, Å., (translated by N. Anderson), *Numerical Methods,* Prentice Hall (1974).

Durrell, C., "Metamorphism in the southern Sierra Nevada northeast of Visalia, California", Ph.D. Thesis, University of California, Berkeley (1936).

Evans, A.G. and Jones, R.L., "Evaluation of a fundamental approach for the statistical analysis of fracture", *Journal of the American Ceramic Society, 61,* No 3-4, pp156-160 (1978).

Evans, A.G., "A general approach for the statistical analysis of multiaxial fracture", *Journal of the American Ceramic Society, 61,* No. 7-8, pp303-308 (1978).

Finnie, I., "Waloddi Weibull - 90 years young on June 18, 1977", *Journal of Engineering Materials and Technology,* pp193, (1977).

Freundenthal, A.M., "Statistical approach to brittle fracture", In *Fracture,* H. Liebowitz, editor, *2,* Chapter 6, Academic Press (1968).

Goodman, R.E., *Introduction to Rock Mechanics,* John Wiley (1980).

Gorham, D.A. and Rickerby, D.G., "A hydraulic strength test for brittle samples", *Journal of Physics E, 8,* pp794-796 (1975).

Griffith, A.A., "The phenomena of rupture and flow in solids", *Philosophical Transactions of the Royal Society,* 221A, pp163-198 (1921).

Griffith, A.A., "The theory of rupture", *Proceedings of the First International Congress on Applied Mechanics,* Delft, pp55-63 (1924).

Gumbel, E.J., *Statistics of Extremes,* Columbia University Press (1958).

Handbook of Molded and Extruded Rubber, The Goodyear Tire and Rubber Company, Inc., Akron, Ohio (1949).

Haimson, B.C., "Hydraulic fracturing in porous and nonporous rock and its potential for determining in-situ stresses at great depth", Missouri River Division Corps of Engineers, *Technical Report no. 4-68* (1968).

Handin, J., "Studies in rock mechanics", Center for Tectonophysics, Texas A&M University, *AD689578,* (1969).

Hardy, M. *et al*, "The failure of rock beams", Part I and II, *International Journal of Rock Mechanics and Mining Science, 10,* pp53-82 (1973).

Hardy, R.H., Jr. and Leighton, F.W., editors, *First Conference on Acoustic Emission and Microseismic Activity in Geological Structures and Materials,* Pennsylvania State University, Trans Tech Publ. (1978).

Hardy, R.H., Jr. and Leighton, F.W., editors, *Second Conference on Acoustic Emission and Microseismic Activity in Geological Structures and Materials,* Pennsylvania State University, Trans Tech Publ. (1980).

Heuze, F.E., "Scale effects in the determination of rock mass strength and deformability", *Rock Mechanics, 12,* No. 3-4, pp167-192 (1980).

Hoskins, E.R., "The failure of thick-walled hollow cylinders of isotropic rock", *International Journal of Rock Mechanics and Mining Science,* Vol. 6, pp99-125 (1969).

Hudson, J.A. and Fairhurst, C., "Tensile strength, Weibull's theory and a general statistical approach to rock failure", In *Proceedings of the Southampton 1969 Civil Engineering* Materials Conference Wiley-Interscience (1969).

Irwin, G.R., "Fracture dynamics", in *Fracture of Metals,* American Society of Metals, Cleveland, pp147-166 (1948).

Jayatilaka, A.Des. and Trustrum, K., "Statistical approach to brittle fracture", *Journal of Materials Science, 12,* pp1426-1430 (1977).

Lundborg, N., "The strength-size relation of granite", *International Journal of Rock Mechanics and Mining Science, 4,* pp269-272 (1967).

McClintock, F.A., "Statistics of brittle fracture", In *Fracture Mechanics of Ceramics,* R.C. Brandt, P.H. Hasselman and F.F. Lange, editors, *1,* Chapter 1, Plenum Press (1977).

McClintock, F.A. and Mayson, H.J., "Principal stress effects on brittle crack statistics", in *The Effects of Voids on Material Deformation,* S.C. Cowin and M.M. Carroll, editors, ASME AMD, *16,* pp31-45 (1976).

Olkiewicz, A., Gale, J.E., Thorpe, R. and Paulsson, B., "Geology and fracture system at Stripa", Lawrence Berkeley Laboratory, *LBL-8907,* (1979).

Pankow, D.H., "The size effect in statistical fracture", D.Eng. Dissertation, University of California, Berkeley (1978).

Pratt, H.R., Black, A.D., Brown, W.D. and Brace, W.F., "The effect of specimen size on the mechanical properties of unjointed diorite", *International Journal of Rock Mechanics and Mining Science,* Vol. 9, No. 4, pp513-530 (1972).

Ralston, A., *A First Course in Numerical Analysis,* McGraw-Hill (1965).

Rice, J.R., "Path independent integral and the approximate analysis of strain concentration by notches and cracks", *Journal of Applied Mechanics, 90,* pp379-386 (1968).

Robinson, E.Y., "The statistical nature of fracture", *UCRL-50622,* Lawrence Livermore

Laboratory, (1970).

Robinson, E.Y. and Finnie, I., "On the statistical interpretation of laboratory tests on rock", *Proceedings of Colloque de Geotechnique,* Toulouse, France, pp1.87-1.118 (1969).

Sundae, L.S., "Effect of specimen volume on apparent tensile strength of three igneous rocks", U.S. Bureau of Mines, *Report of Investigations 7846,* (1974).

Swan, G., "Some observations concerning the strength-size dependency of rocks", *Research Report TULEA 1980:01,* Luleå, Sweden (1980a).

Swan, G., "Fracture stress scale effects for rocks in bending", *International Journal of Rock Mechanics and Mining Science,* Vol 17, pp317-324 (1980b).

Timoshenko, S.P. and Goodier, J.N., *Theory of Elasticity,* McGraw-Hill (1970).

Timoshenko, S. and Lessels, J.M., *Applied Elasticity,* Westinghouse Technical Night School Press (1925).

Vardar, O., "Fracture of brittle solids under multiaxial and dynamic loading", Ph.D. Thesis, University of California, Berkeley (1975).

Vardar, O. and Finnie, I., "An analysis of the Brazilian disc fracture test using the Weibull probabilistic treatment of brittle strength", *International Journal of Fracture, 11,* pp495-508 (1975).

Volkov, S.D., *Statistical Strength Theory,* (Translated from the Russian Edition), Gordon and Breach (1962).

Weibull, W., "A statistical theory of the strength of materials", *Ingeniorsvetenskap*

Akademiens Handlingar, Nr. 151 (1939a).

Weibull, W., "The phenomena of rupture in solids", *Ingeniorsvetenskap Akademiens Handlingar,* Nr. 153 (1939b).

Wijk, G., Rehbinder, G. and Lögdström, G., "The relation between the uniaxial tensile strength and the sample size for Bohus granite", *Rock Mechanics, 10,* pp201-219 (1978).

Wijk, G., "Some new theoretical aspects of indirect measurements of the tensile strength of rocks", *International Journal of Rock Mechanics and Mining Science,* Vol. 15, pp149-160 (1978).

Zoback, M.D., Rummel, F., Jung, R. and Raleigh, C.B., "Laboratory hydraulic fracturing experiments in intact and pre-fractured rock", *International Journal of Rock Mechanics and Mining Science,* Vol. 14, pp49-58 (1977).

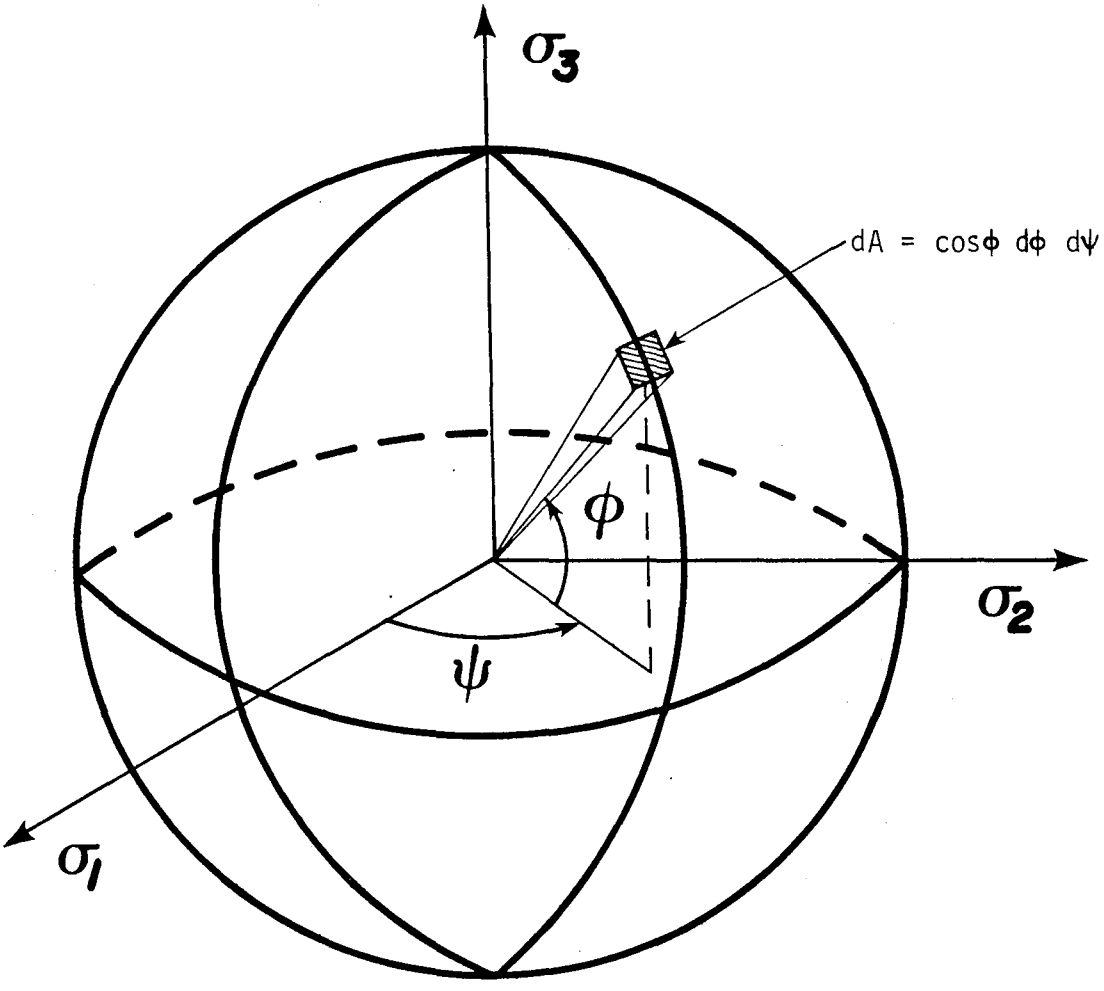

Figure 2-1. Unit Sphere in Principal Stress Space.

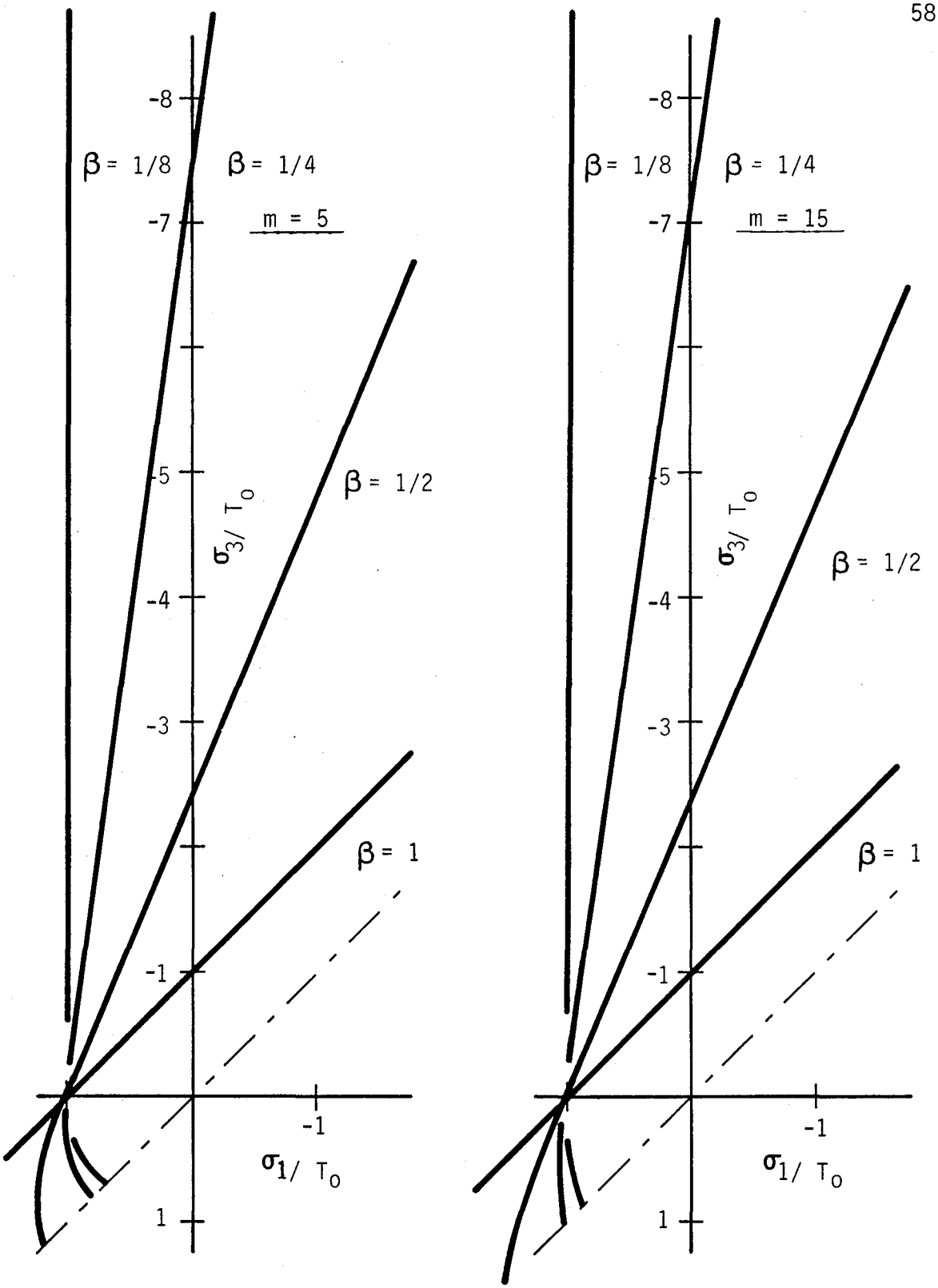

Figure 3-1. Triaxial Fracture Envelope.

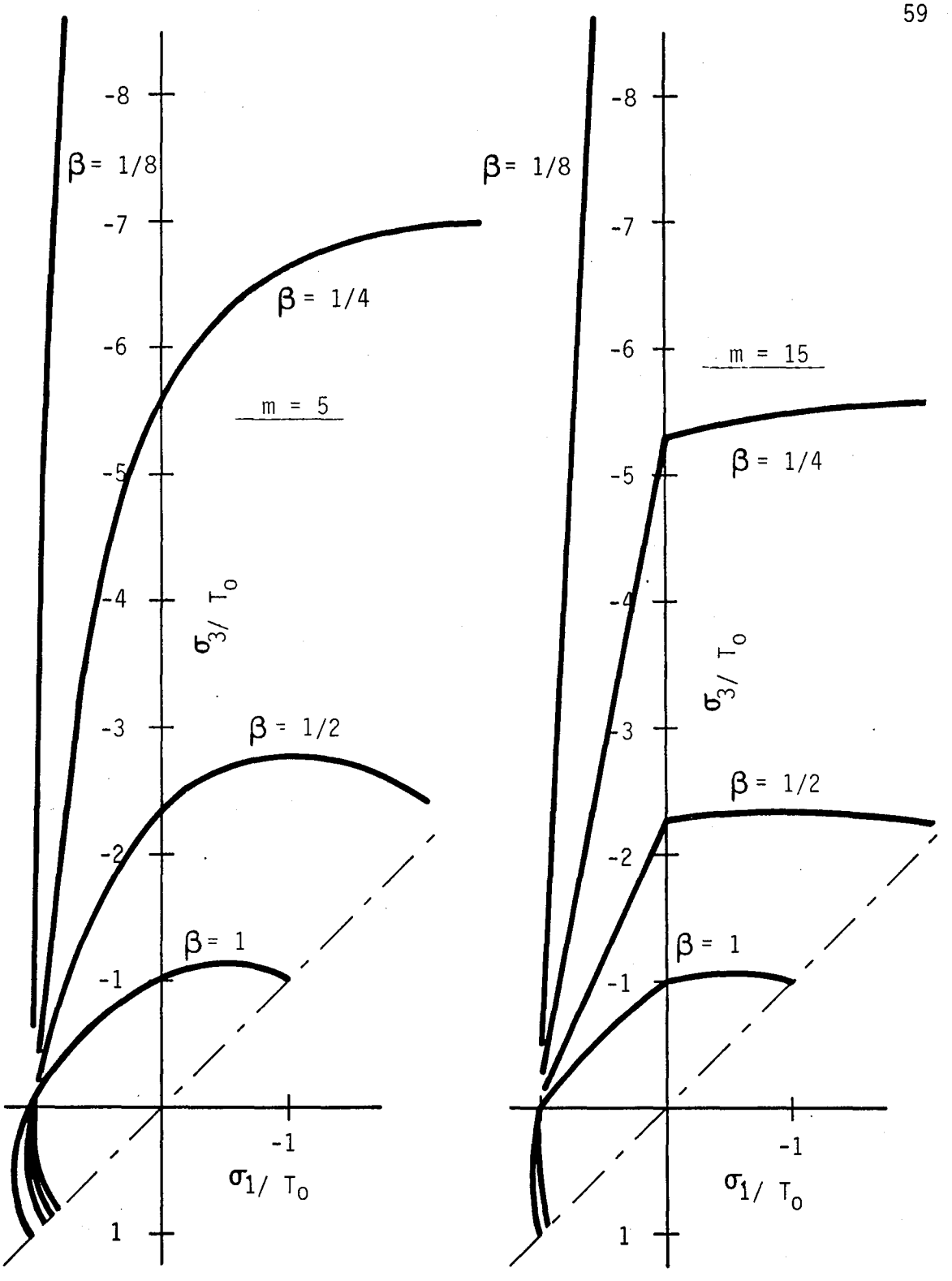

Figure 3-2. Biaxial Fracture Envelope.

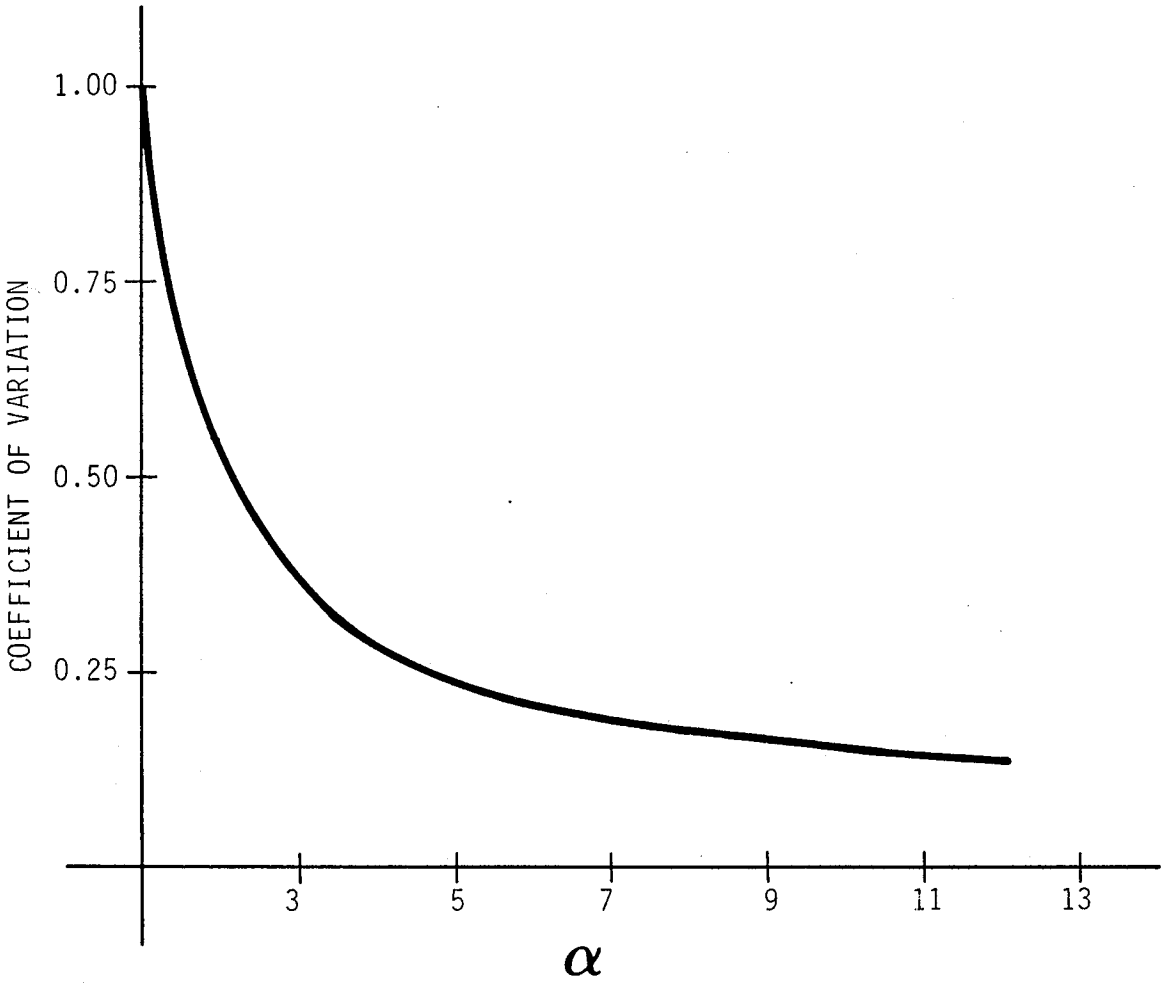

Figure 4-1. Coefficient of Variation as a Function of α for a Two Parameter Weibull Model.

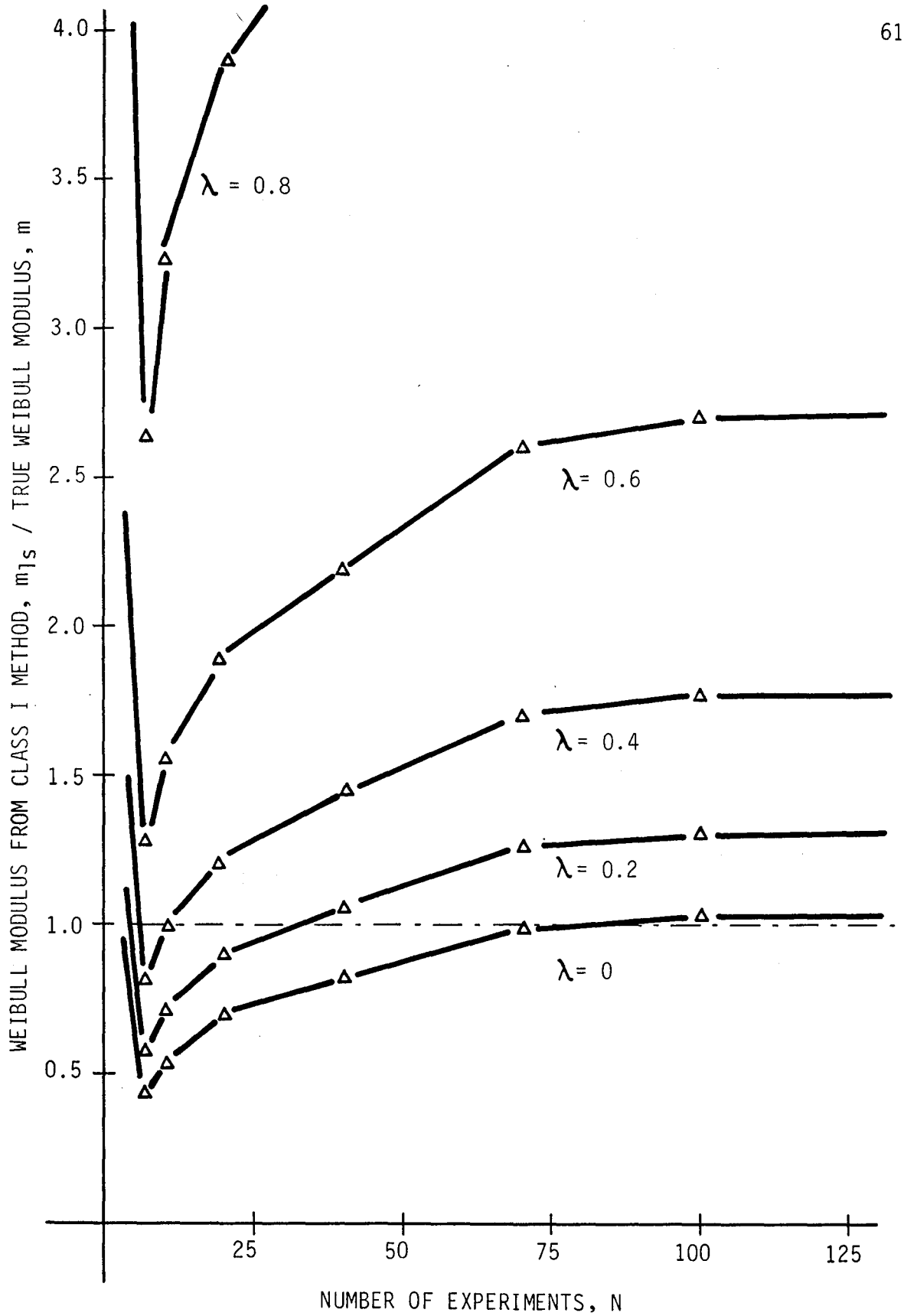

Figure 4-2. Ratio of Weibull Moduli from Class I Method to True Weibull Moduli as a Function of the Number of Tests.

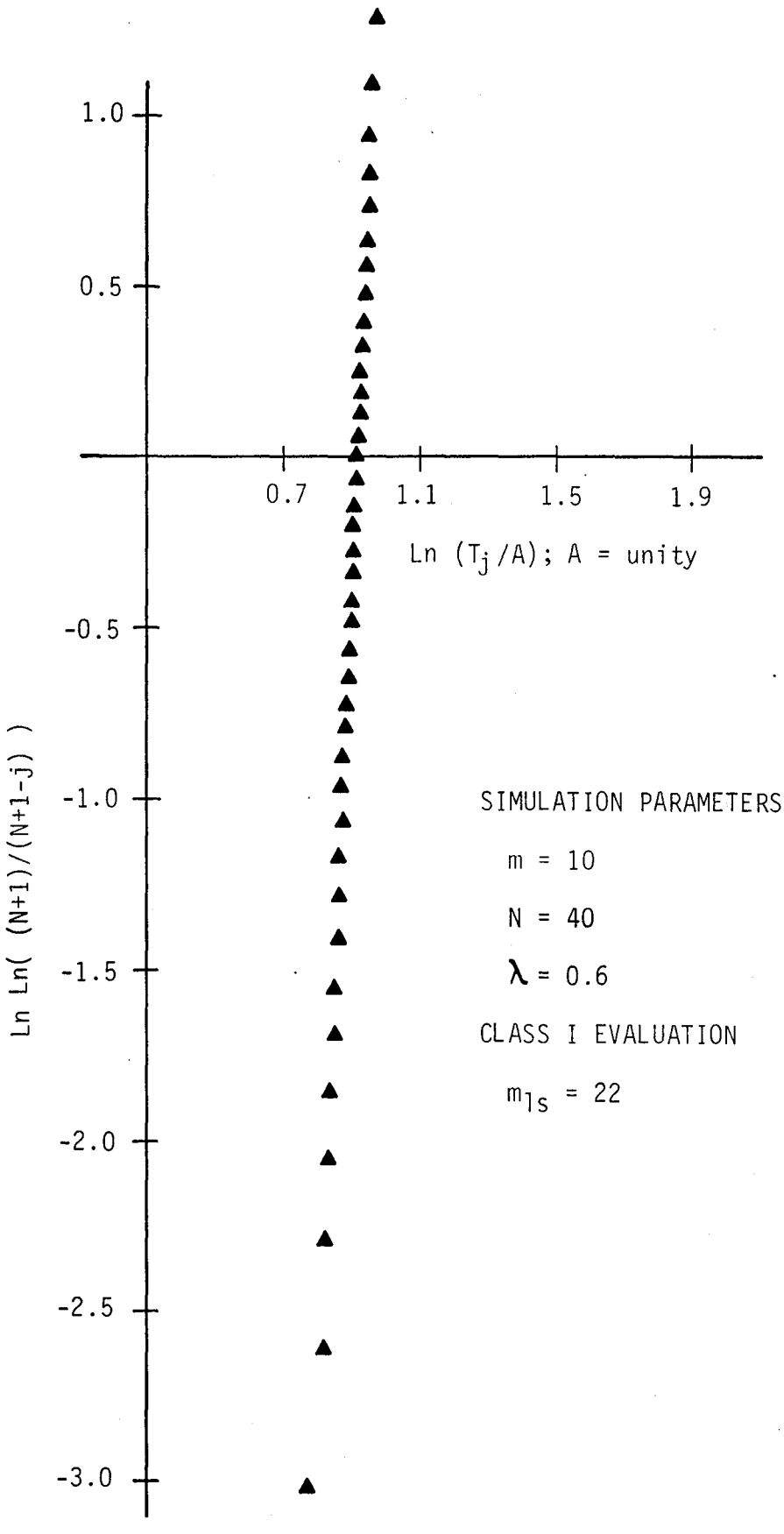

Figure 4-3. Simulated Three Parameter Data in the Space of Equation (4-4).

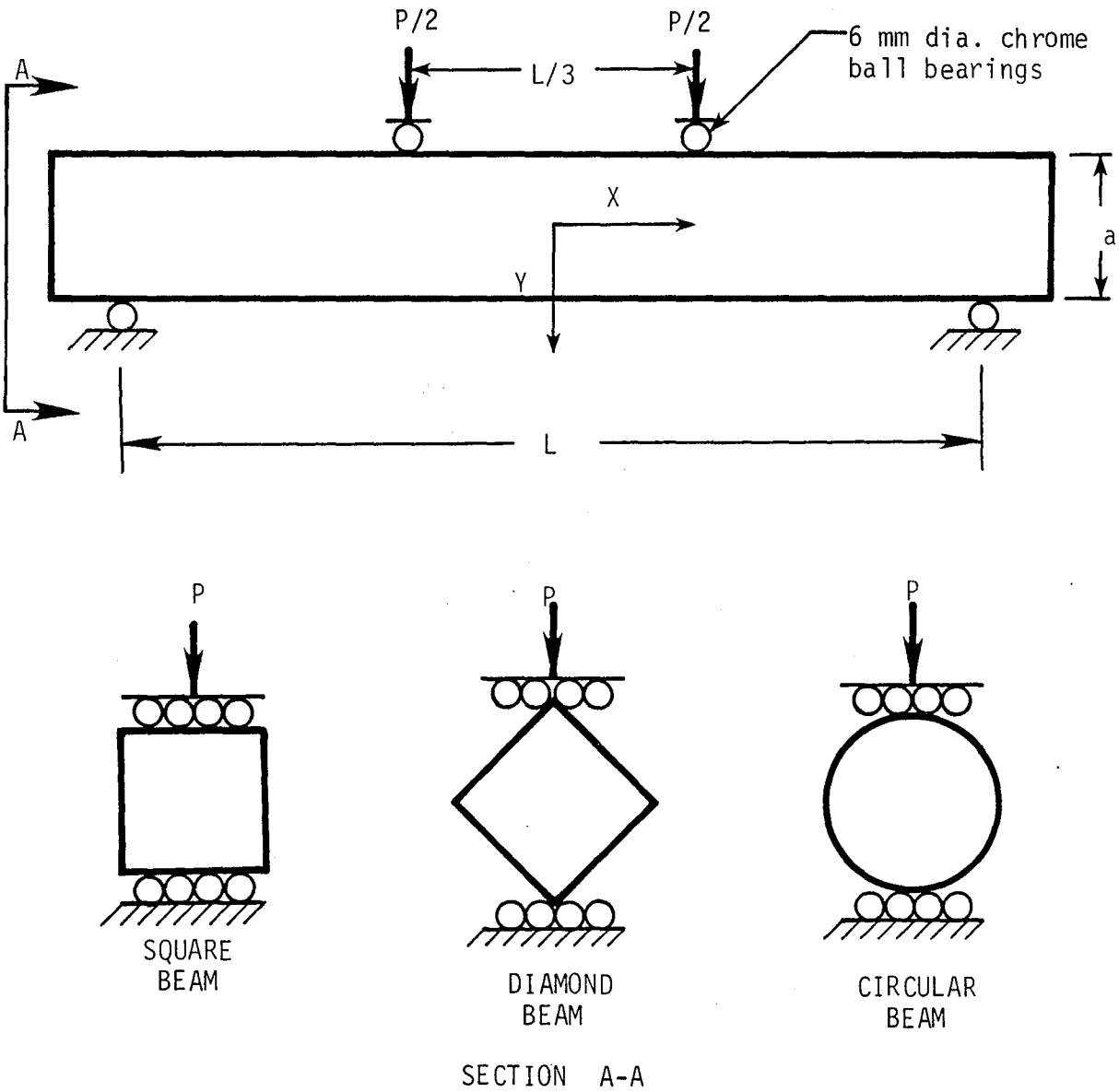

Figure 5-1. Four Point Bending Test.

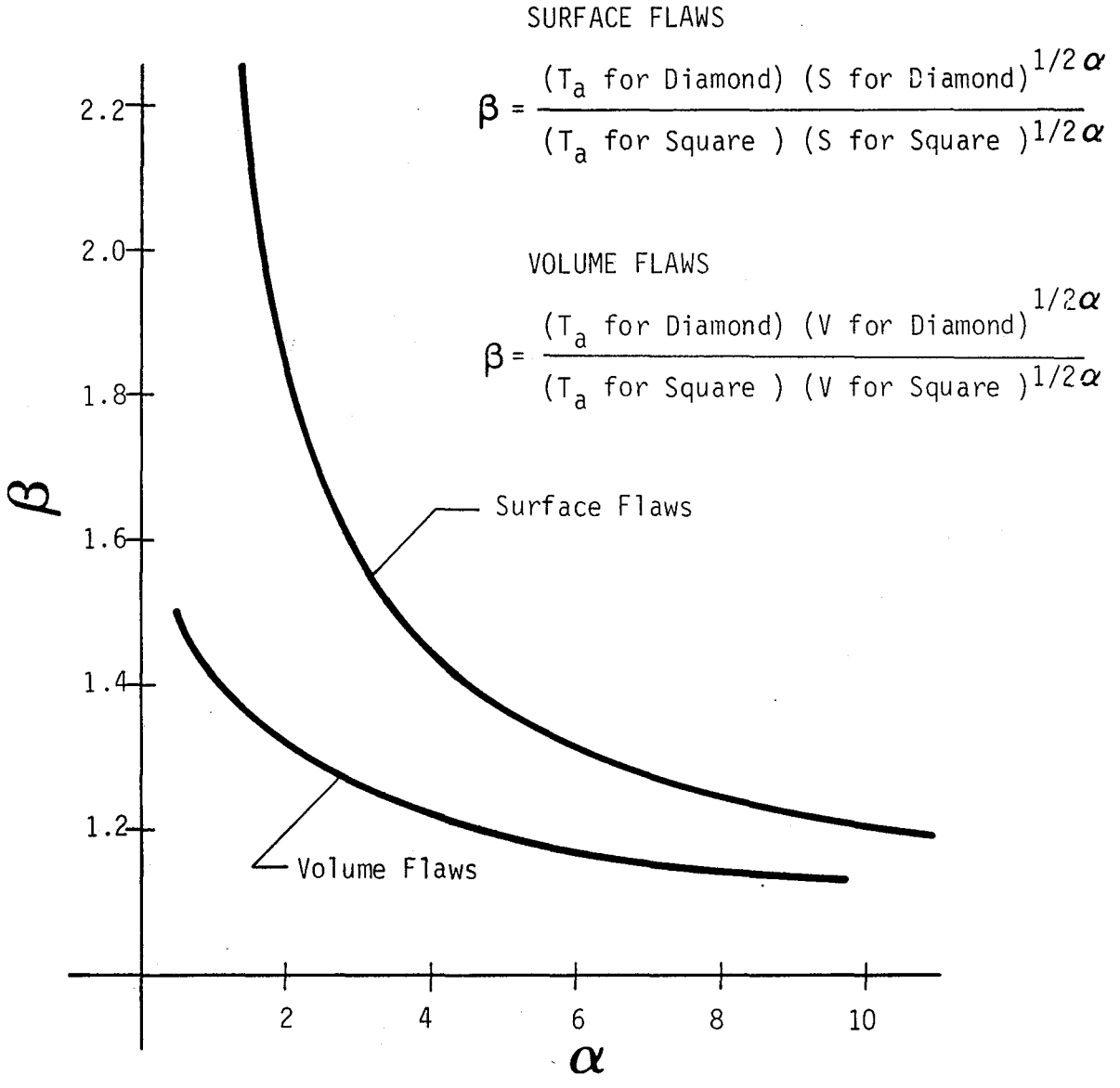

Figure 5-2. Ratio of Mean Apparent Tensile Strength of Diamond Beams to Mean Apparent Tensile Strength of Square Beams for a Two Parameter Weibull Material with Volume or Surface Flaws.

SURFACE FLAWS

$$\beta = \frac{(T_a \text{ for Circular})\ (S \text{ for Circular})^{1/2\alpha}}{(T_a \text{ for Square }\ )\ (S \text{ for Square }\ )^{1/2\alpha}}$$

VOLUME FLAWS

$$\beta = \frac{(T_a \text{ for Circular})\ (V \text{ for Circular})^{1/2\alpha}}{(T_a \text{ for Square }\ )\ (V \text{ for Square }\ )^{1/2\alpha}}$$

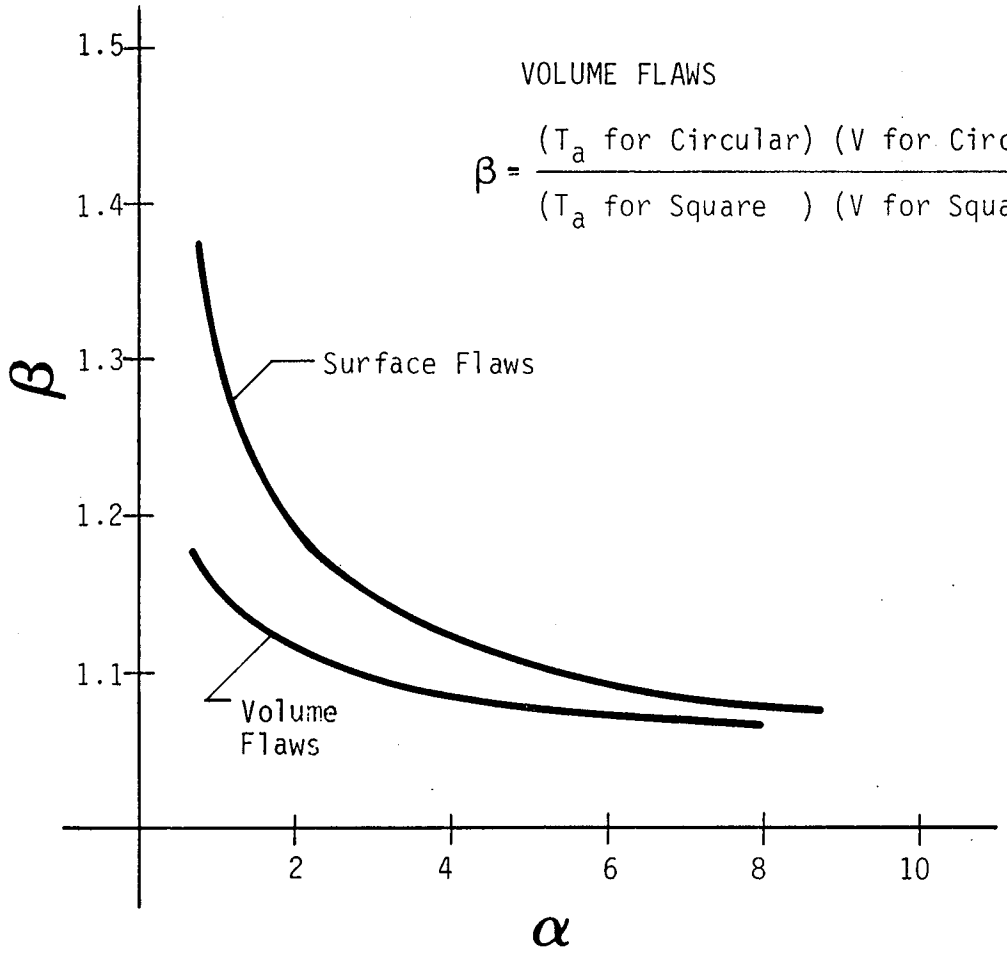

Figure 5-3. Ratio of Mean Apparent Tensile Strength of Circular Beams to Mean Apparent Tensile Strength of Square Beams for a Two Parameter Weibull Material with Volume or Surface Flaws.

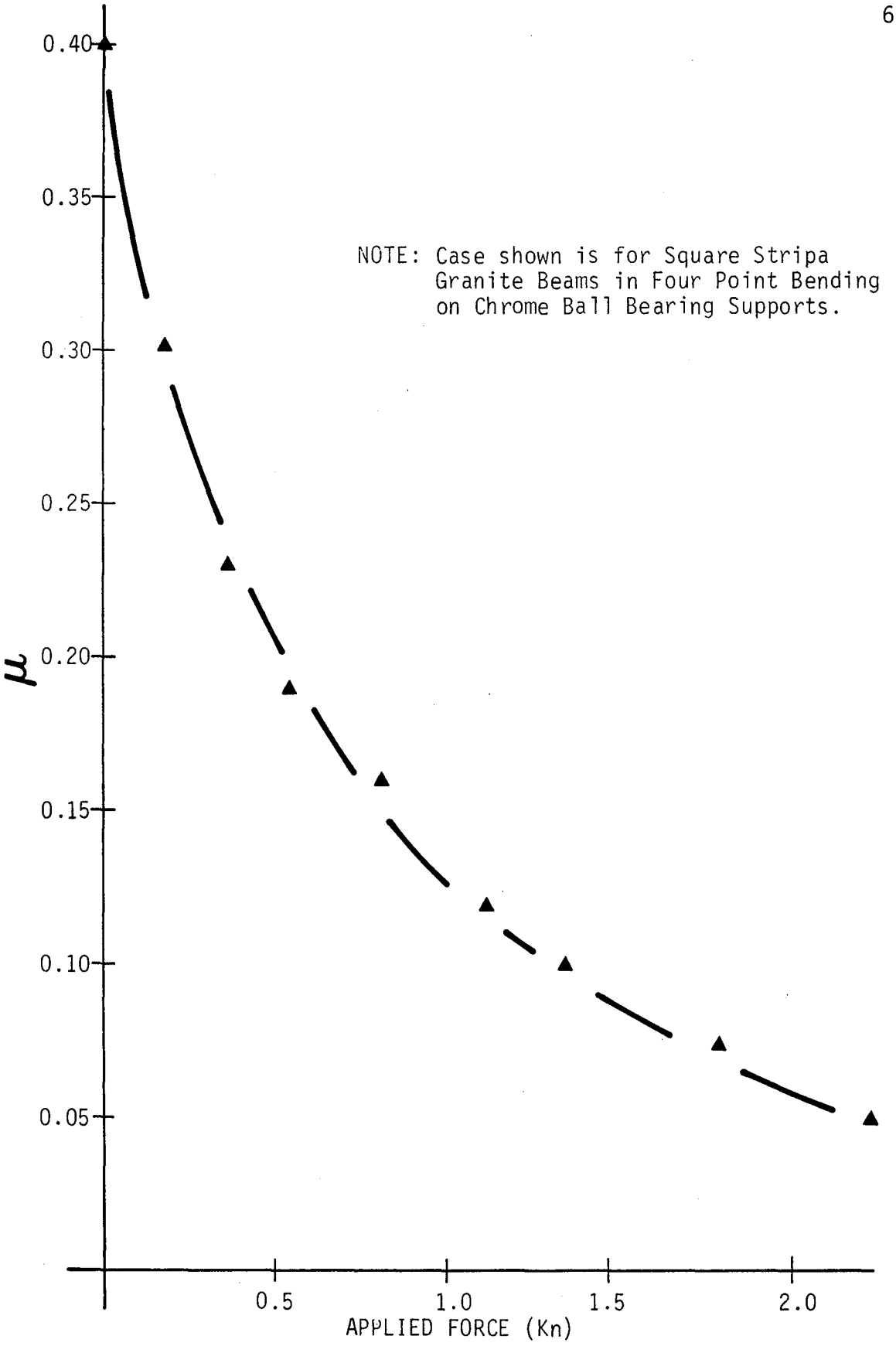

Figure 5-4. Coefficient of Friction as a Function of Applied Load.

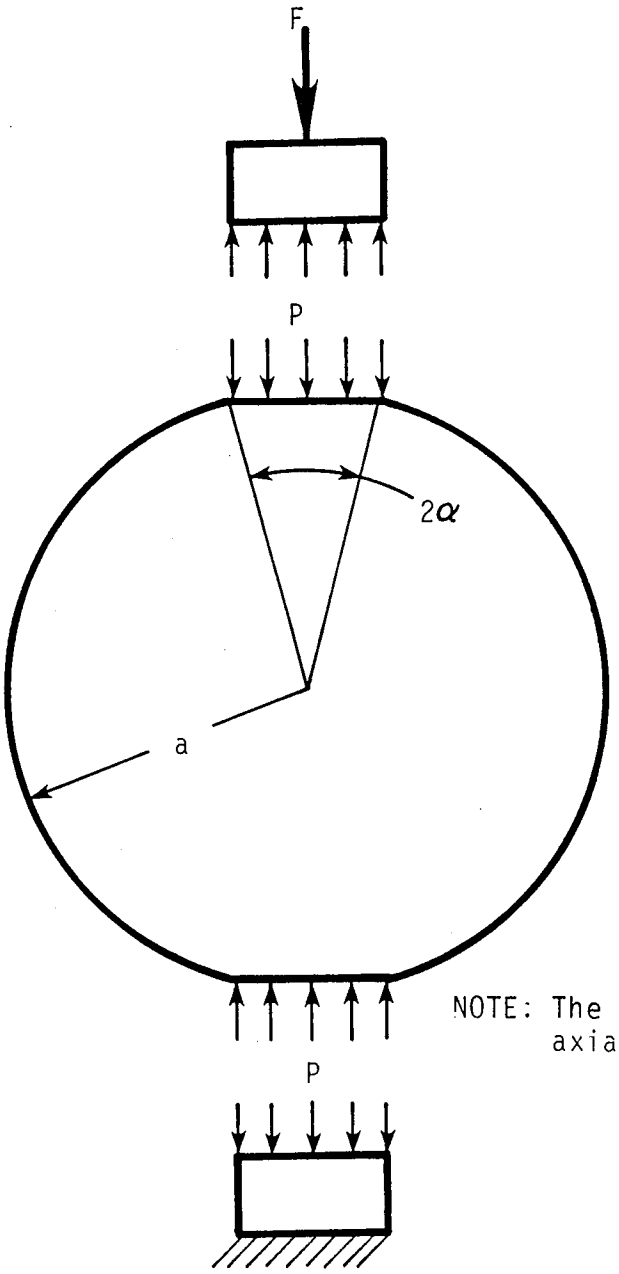

NOTE: The dimension in the axial direction is "t".

Figure 5-5. Brazilian Test.

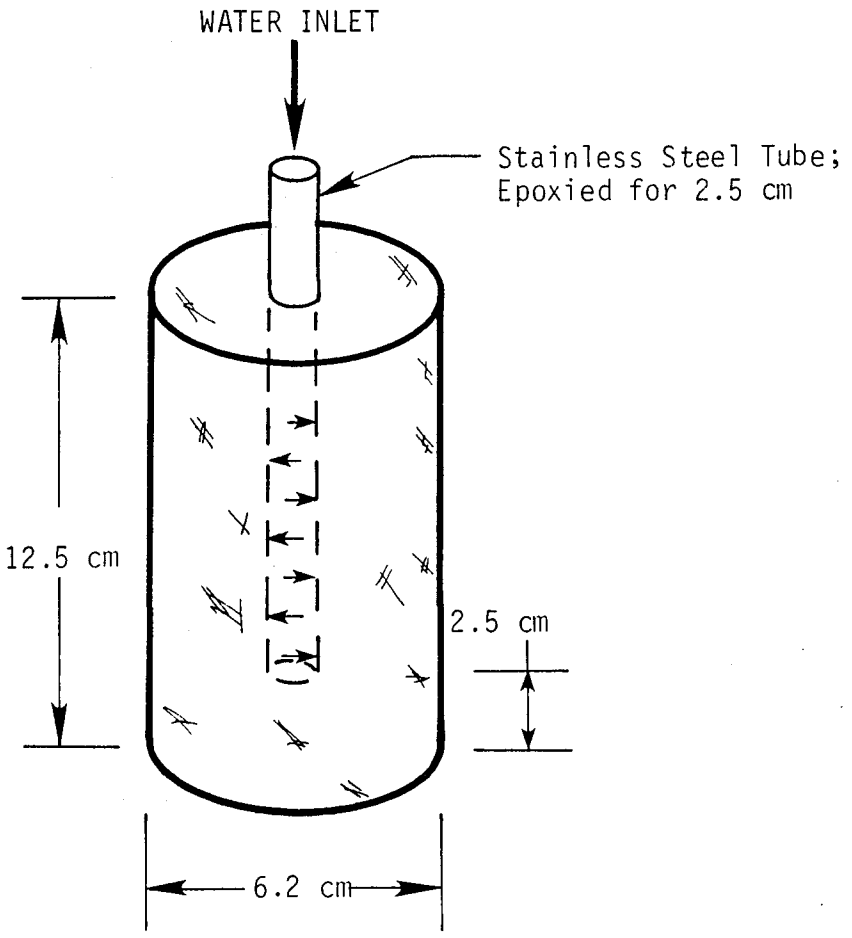

Figure 5-6. Laboratory Hydraulic Fracture Test.

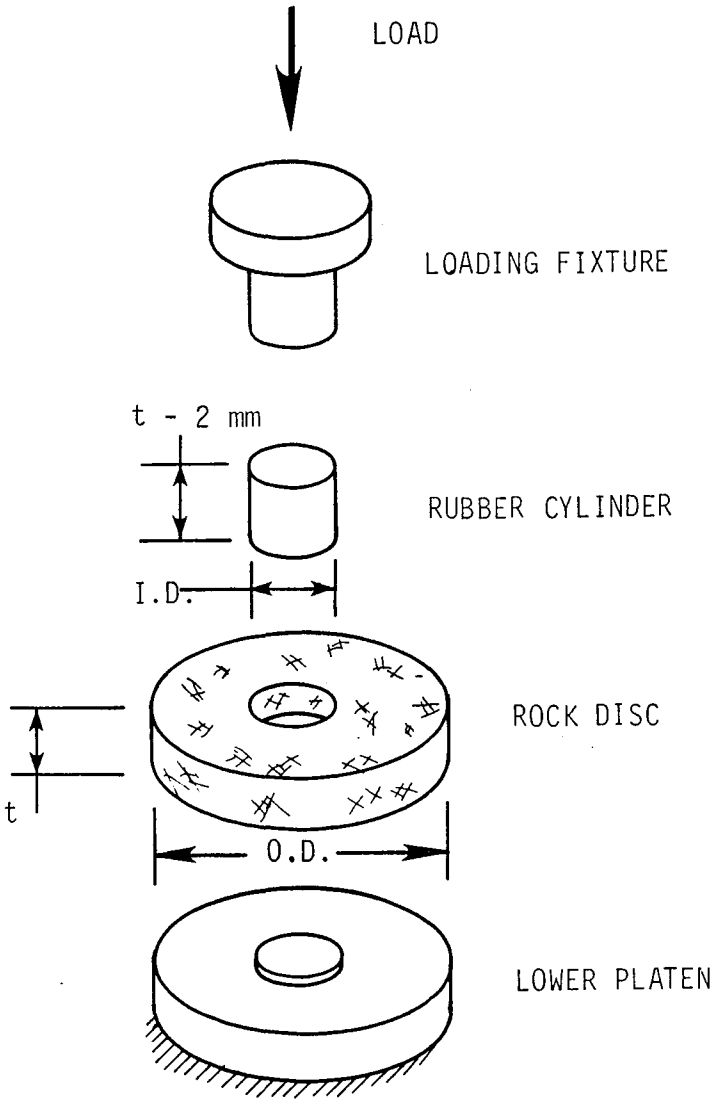

Figure 5-7. Rubber Fracturing Test.

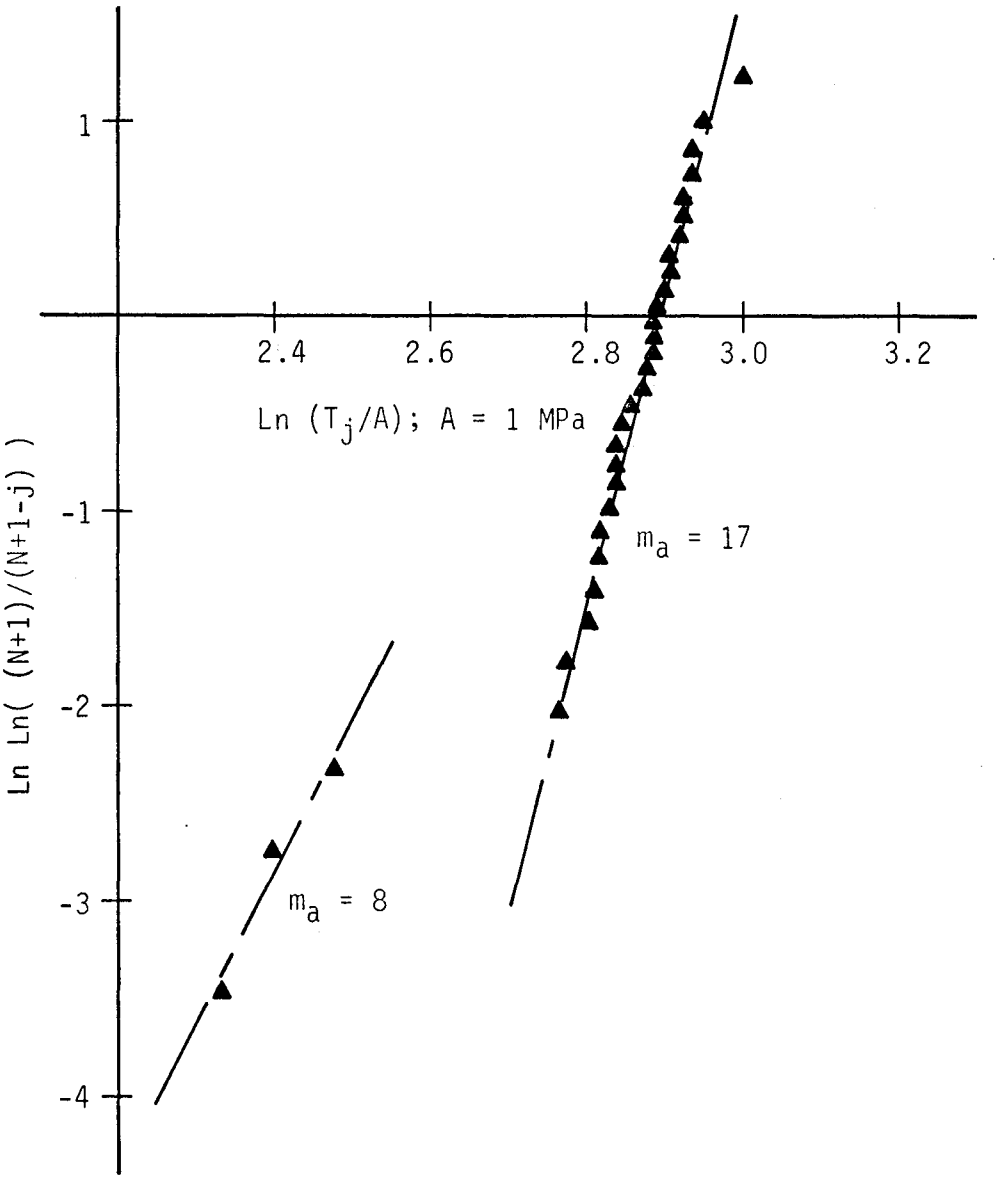

Figure 6-1. Apparent Tensile Strength for Square Beams of Carrara Marble in the Space of Equation (4-4).

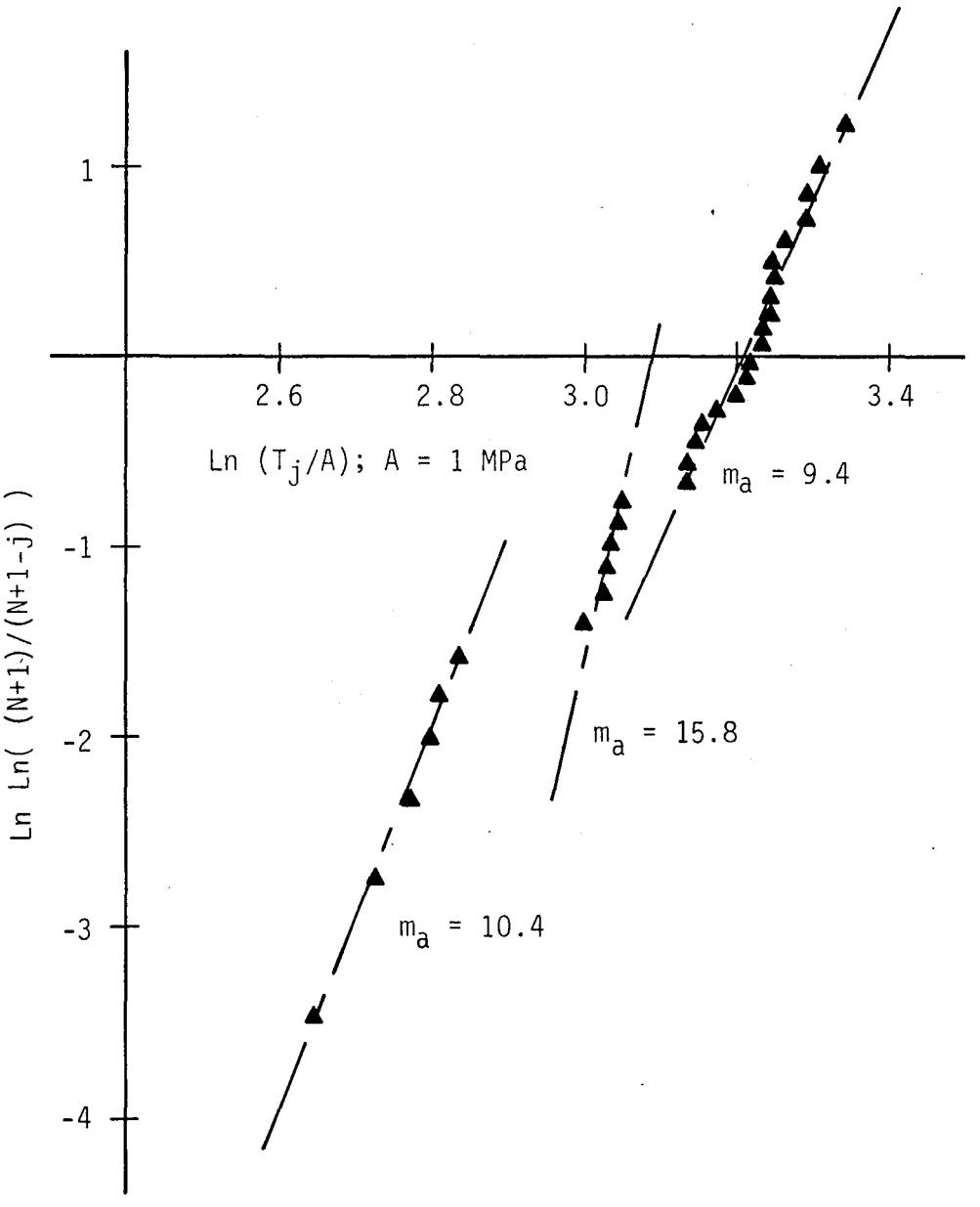

Figure 6-2. Apparent Tensile Strength for Diamond Beams of Carrara Marble in the Space of Equation (4-4).

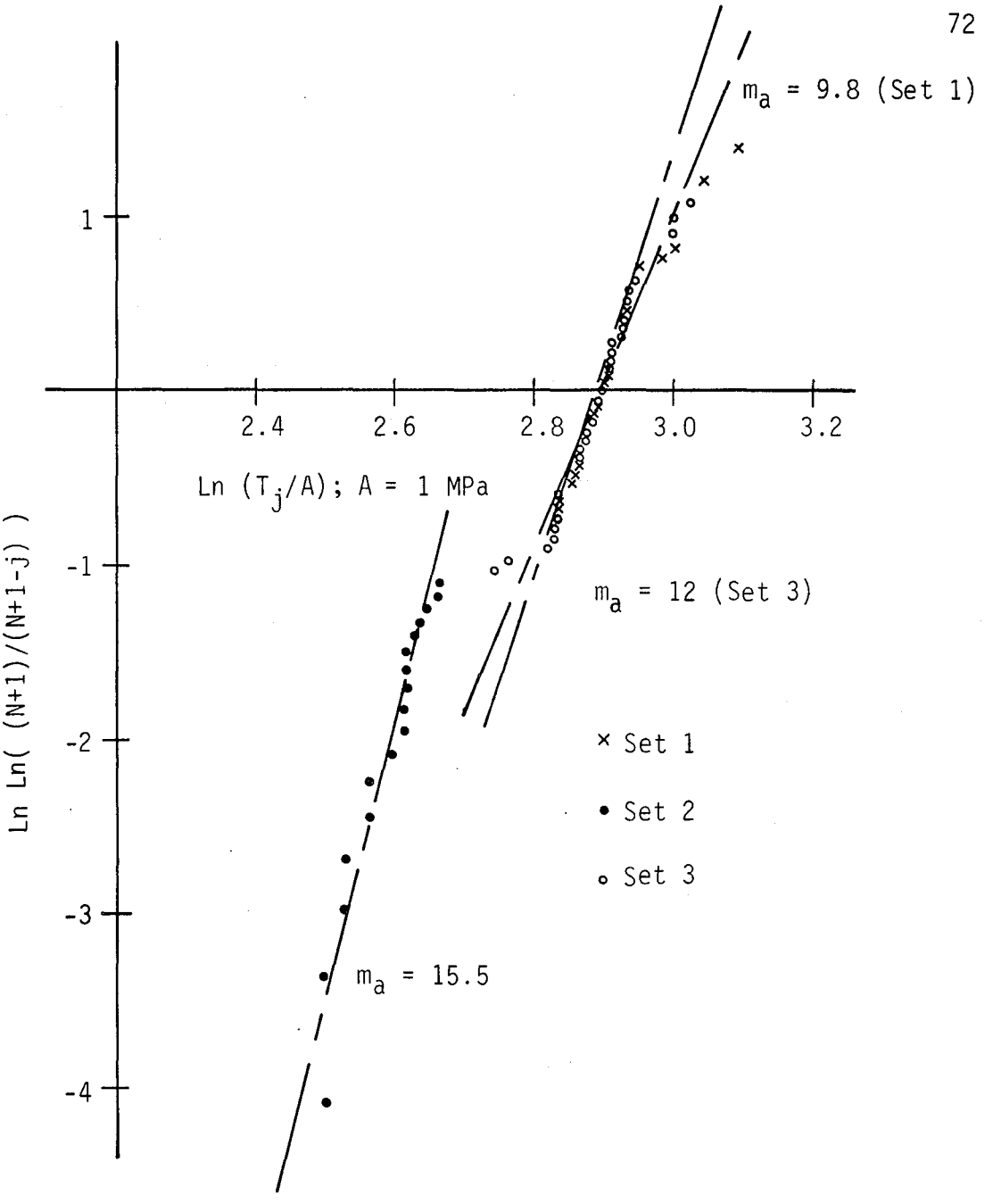

Figure 6-3. Apparent Tensile Strength for Circular Beams of Carrara Marble in the Space of Equation (4-4).

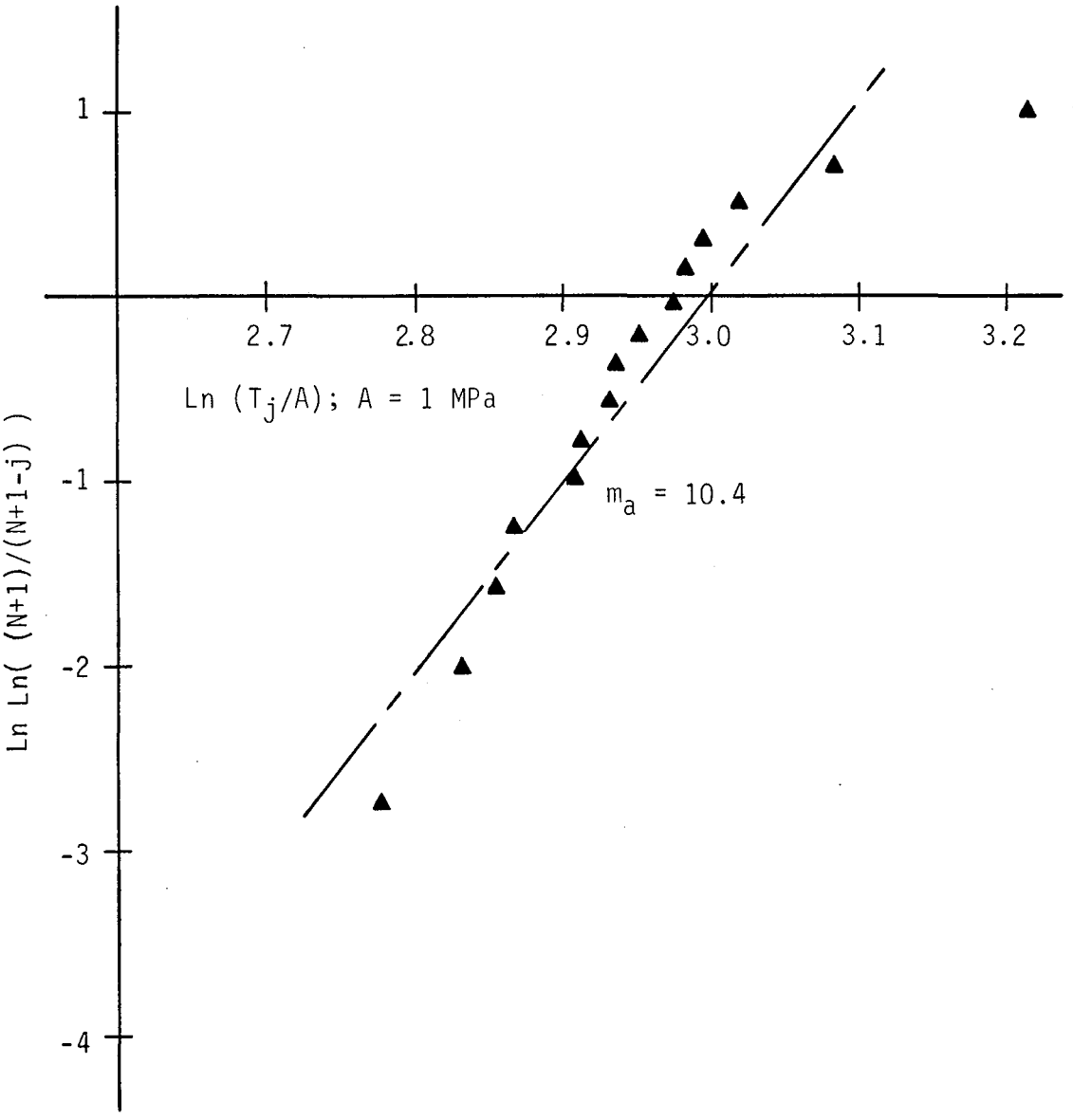

Figure 6-4. Apparent Tensile Strength for Square Beams of Sierra White Granite in the Space of Equation (4-4).

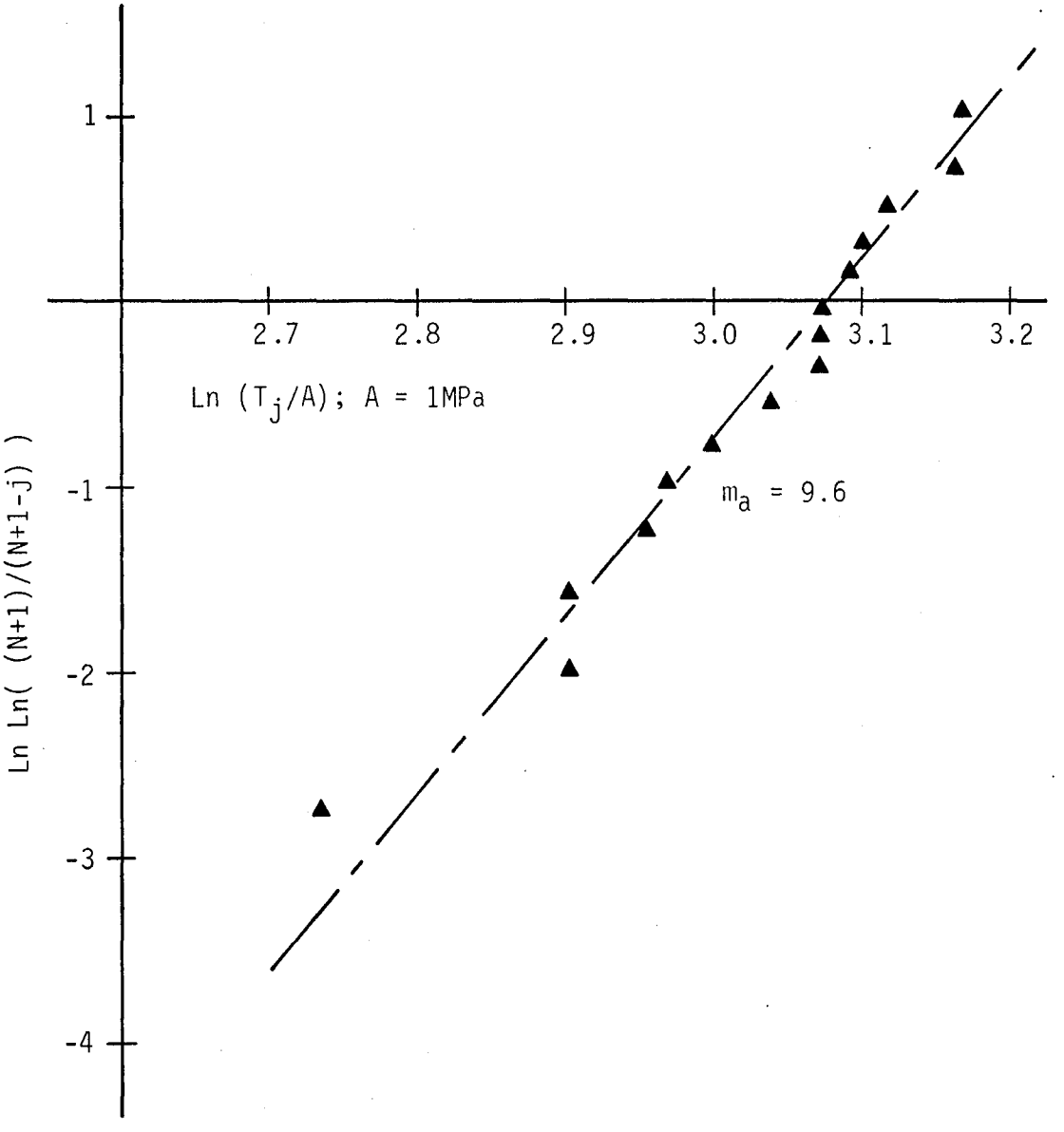

Figure 6-5. Apparent Tensile Strength for Diamond Beams of Sierra White Granite in the Space of Equation (4-4).

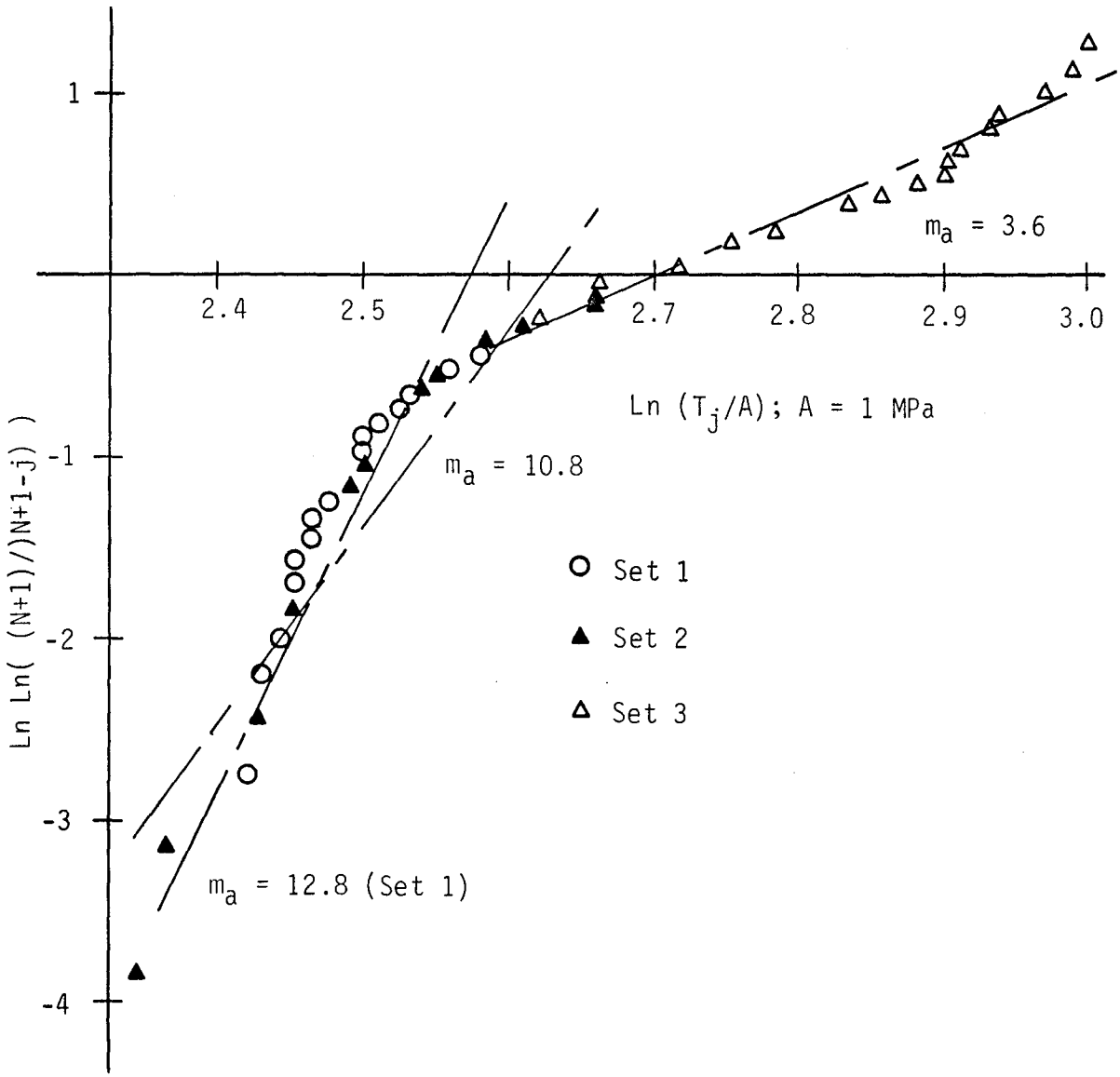

Figure 6-6. Apparent Tensile Strength for Circular Beams of Sierra White Granite in the Space of Equation (4-4).

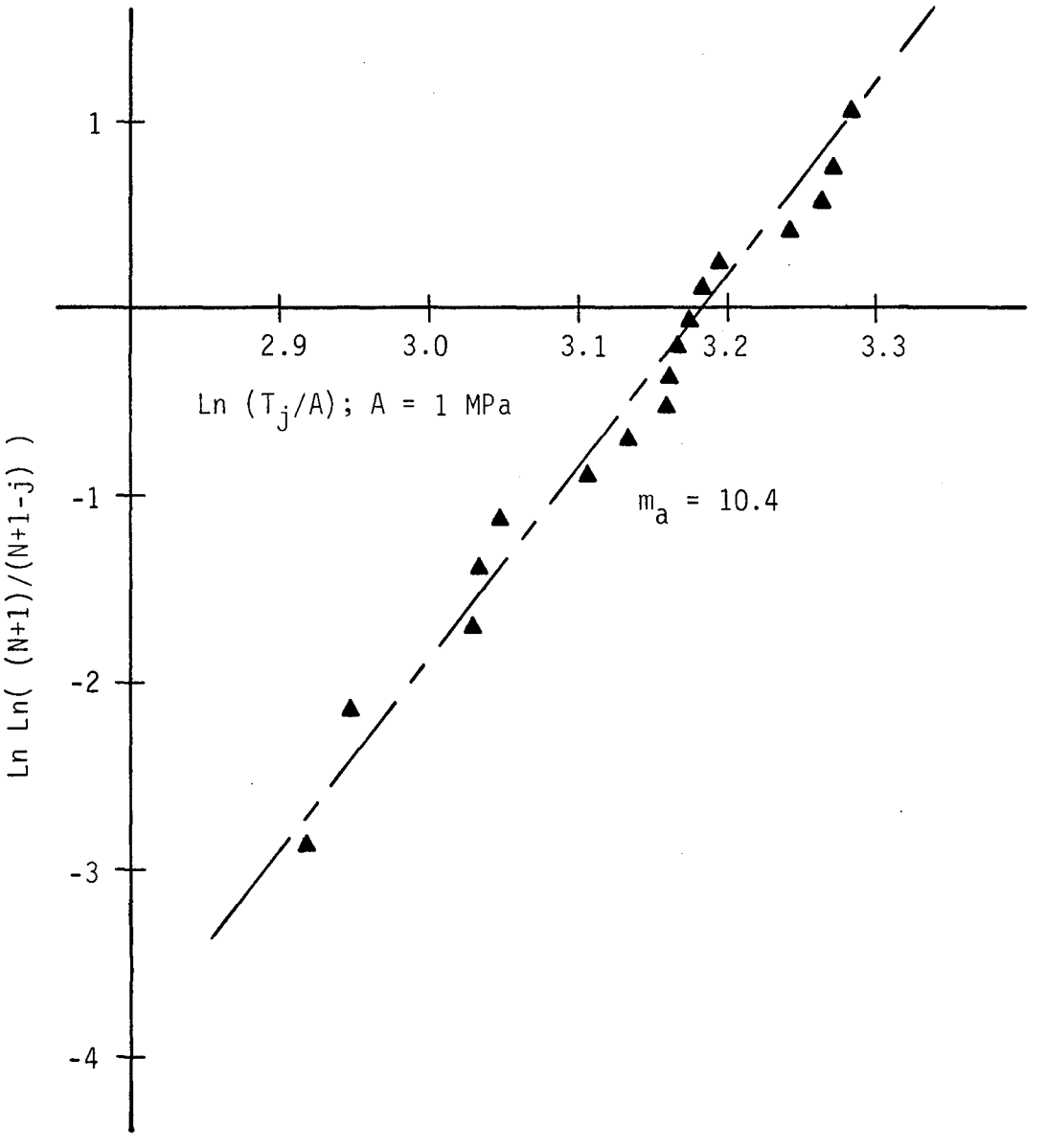

Figure 6-7. Apparent Tensile Strength for Square Beams of Stripa Granite in the Space of Equation (4-4).

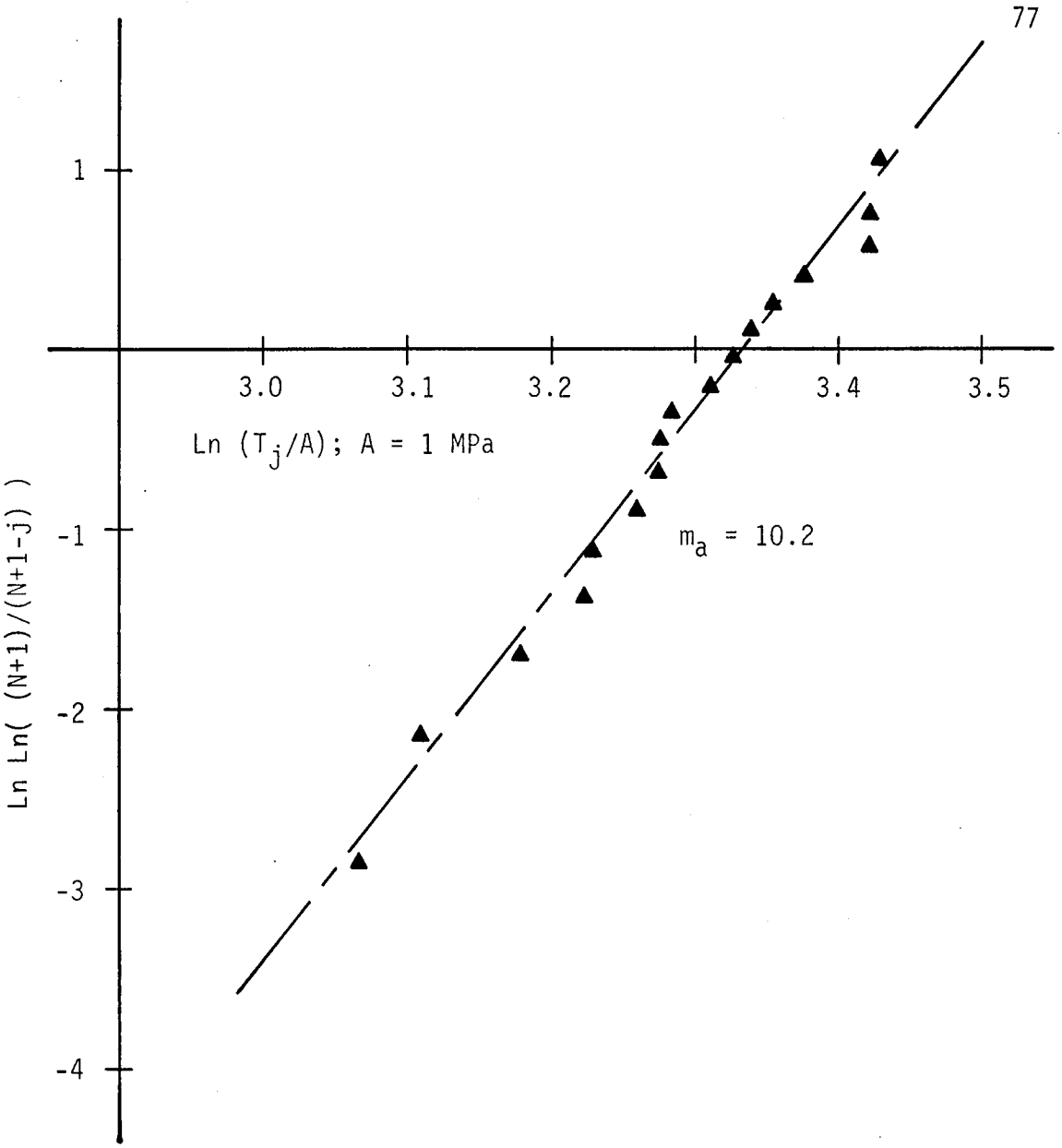

Figure 6-8. Apparent Tensile Strength for Diamond Beams of Stripa Granite in the Space of Equation (4-4).

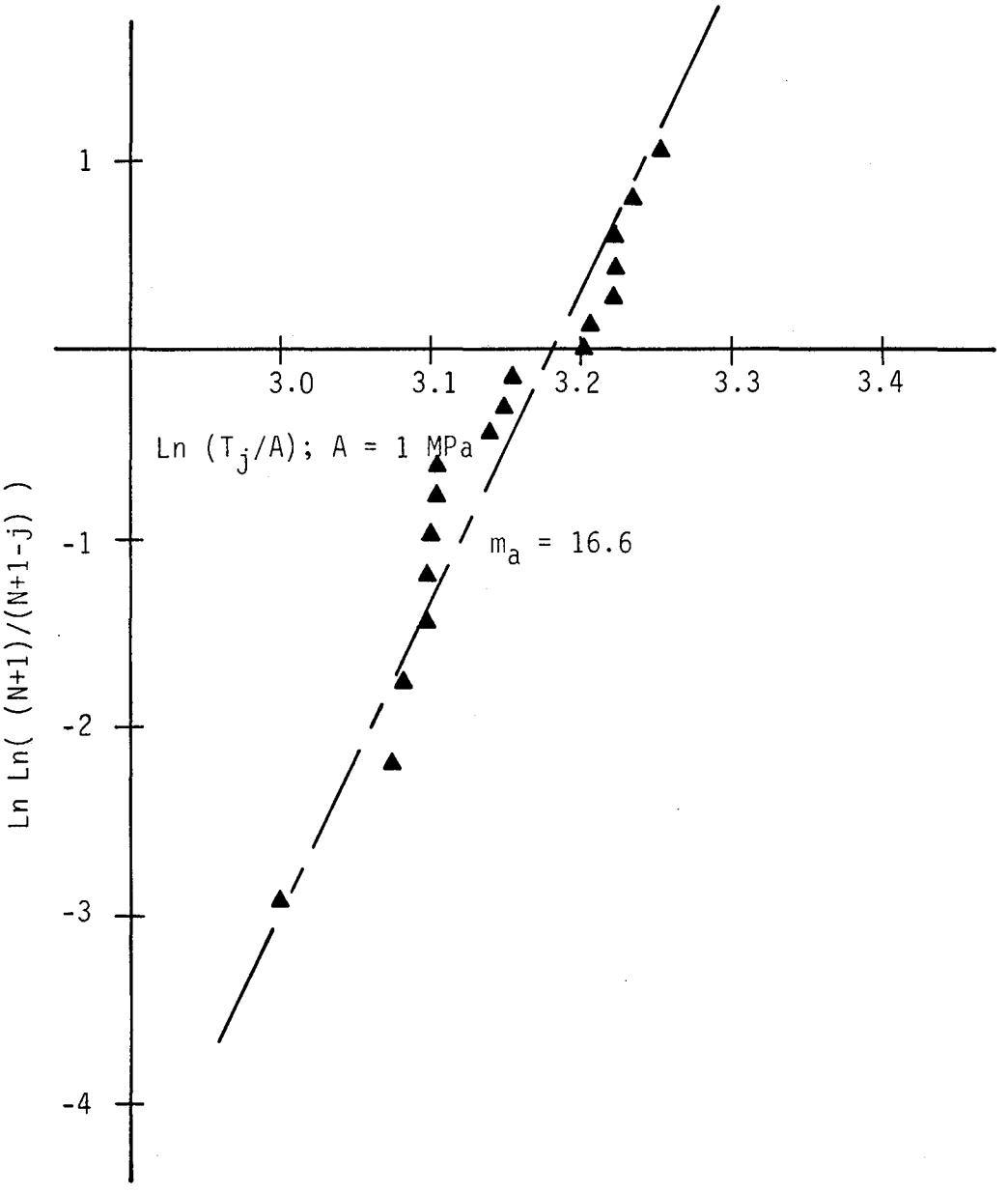

Figure 6-9. Apparent Tensile Strength for Circular Beams of Stripa Granite in the Space of Equation (4-4).

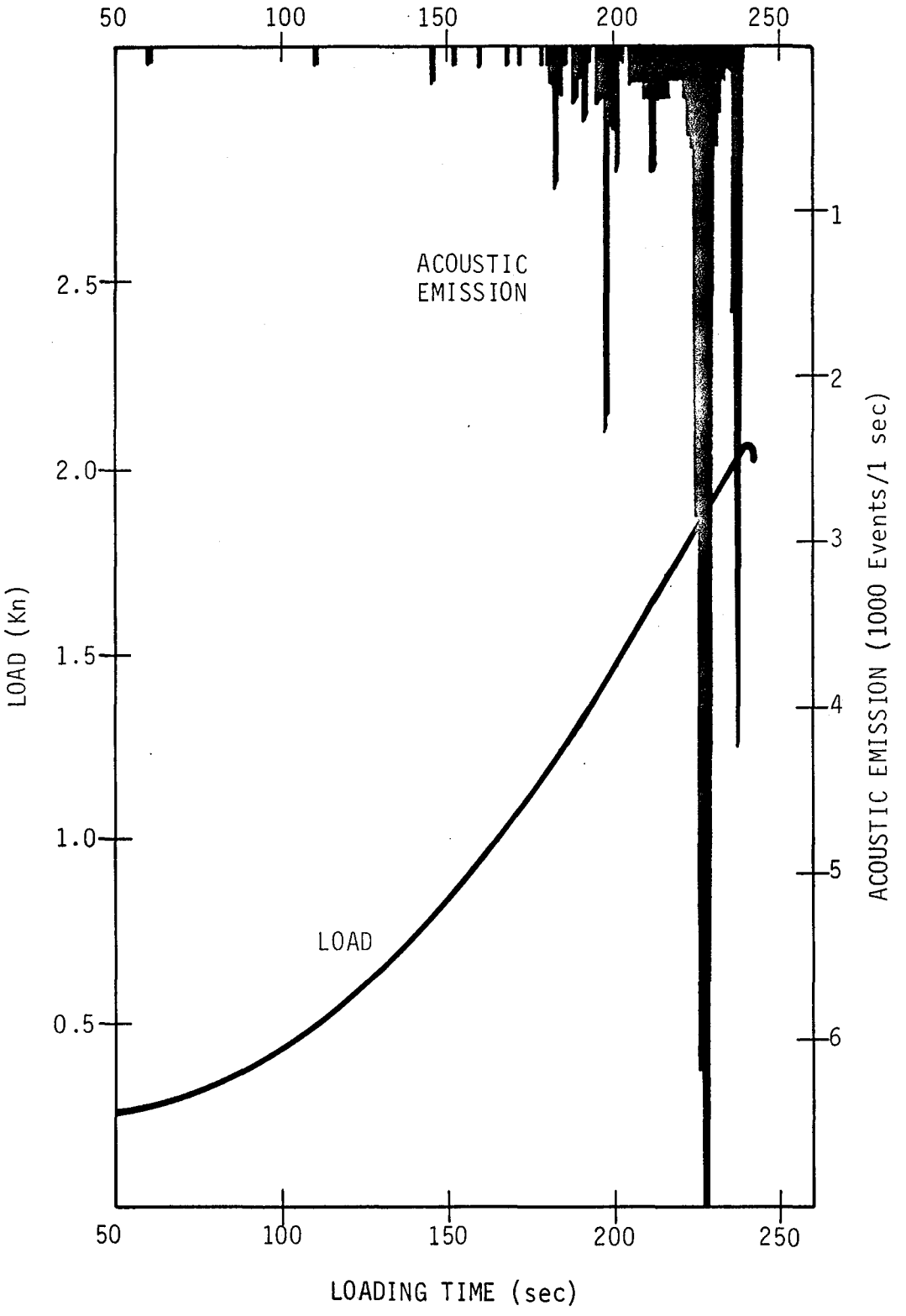

Figure 6-10. Load and Acoustic Emission for a Rubber Fracturing Test of Concrete.

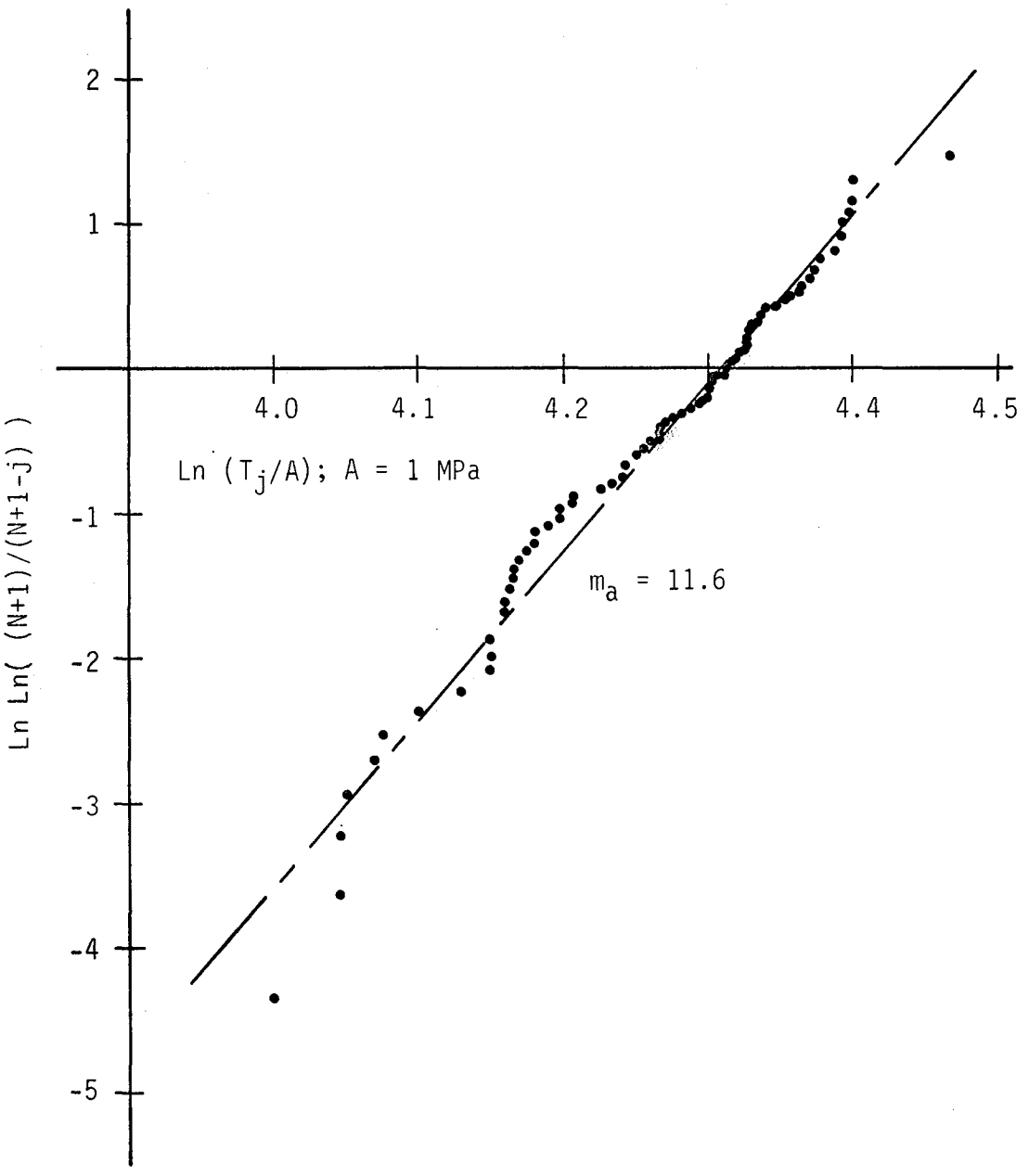

Figure 6-11. Apparent Tensile Strength for Rubber Fracturing Data Sets A and B in the Space of Equation (4-4).

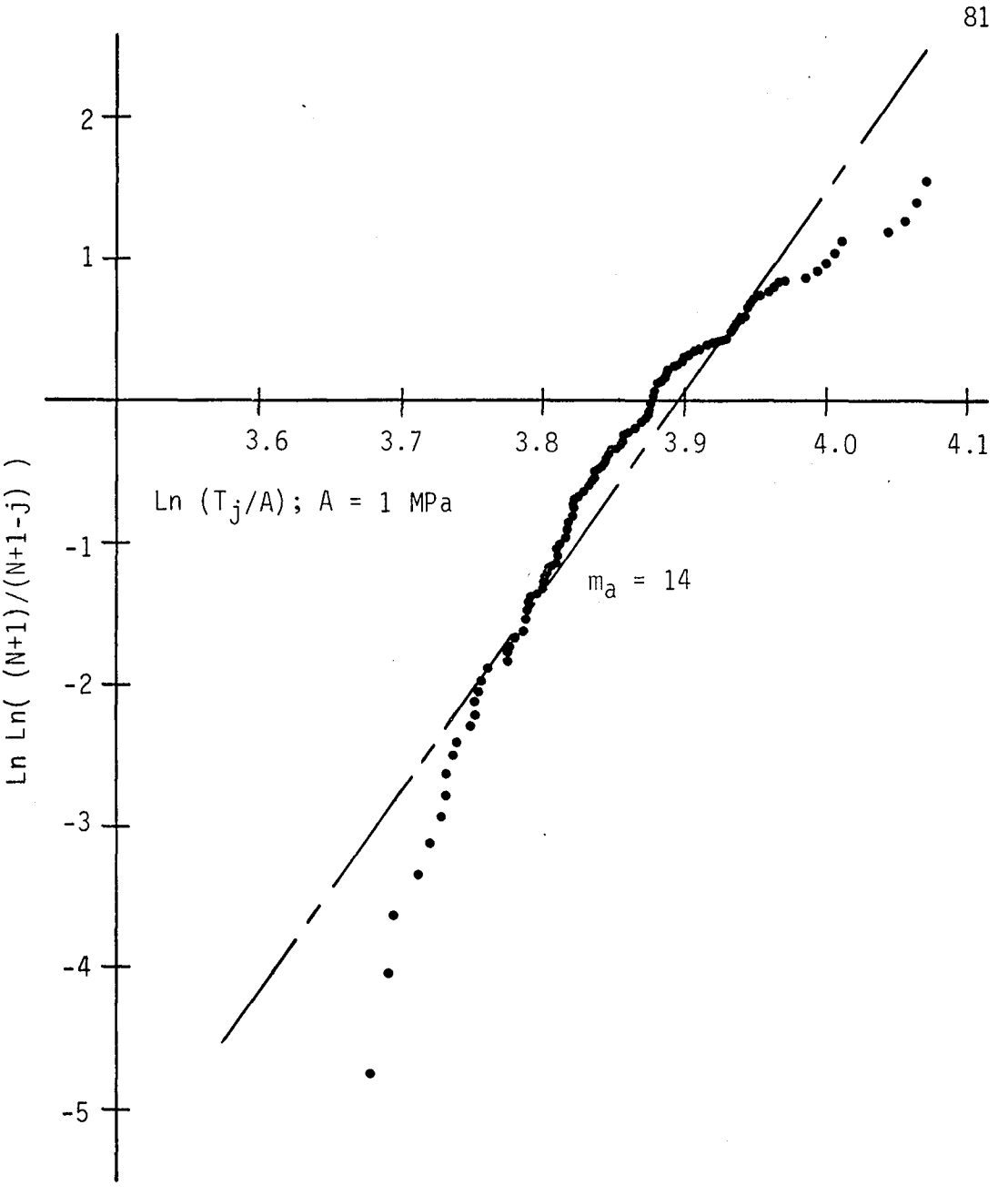

Figure 6-12. Apparent Tensile Strength for Rubber Fracturing Data Sets C and D in the Space of Equation (4-4).

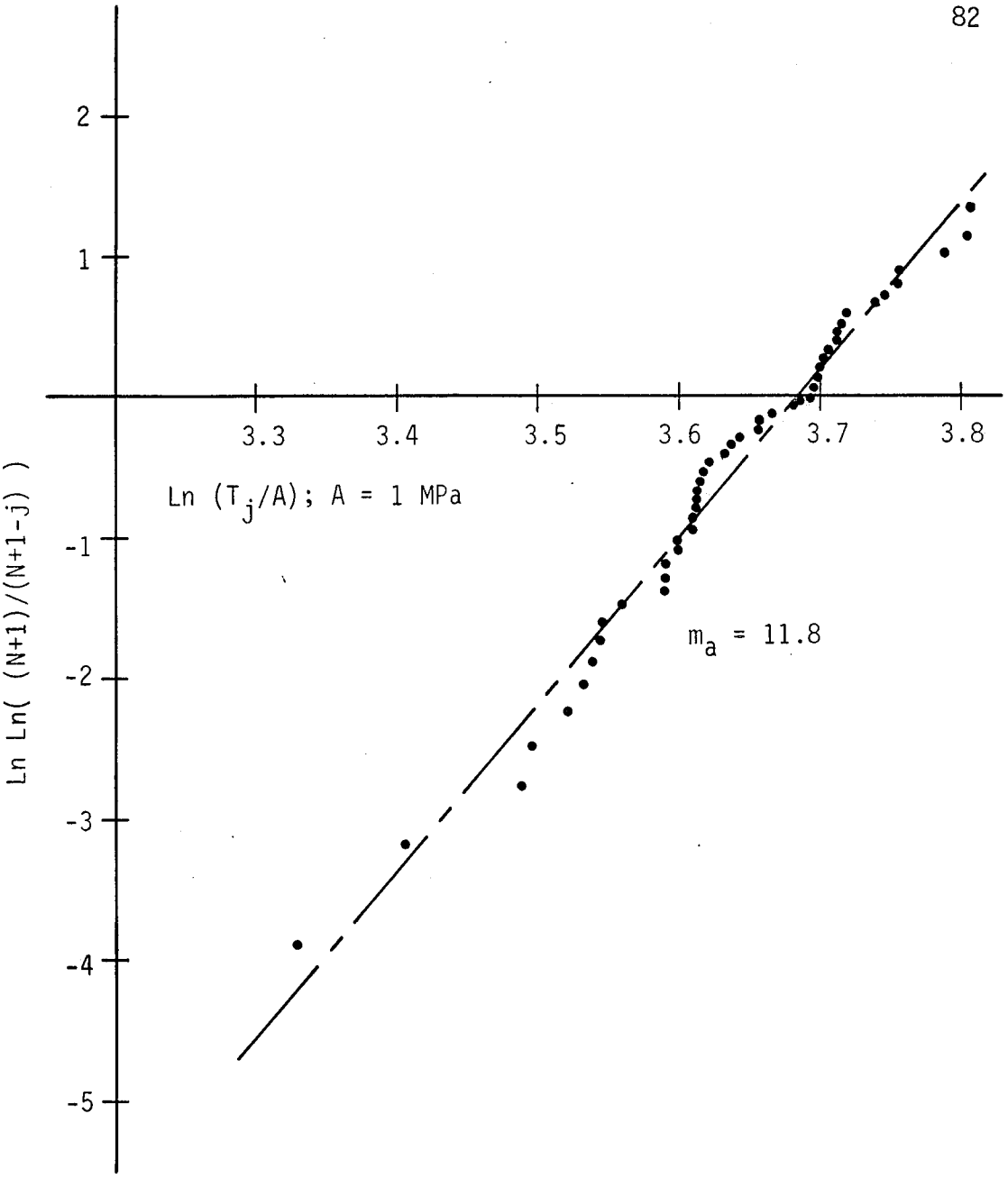

Figure 6-13. Apparent Tensile Strength for Rubber Fracturing Data Sets E and F in the Space of Equation (4-4).

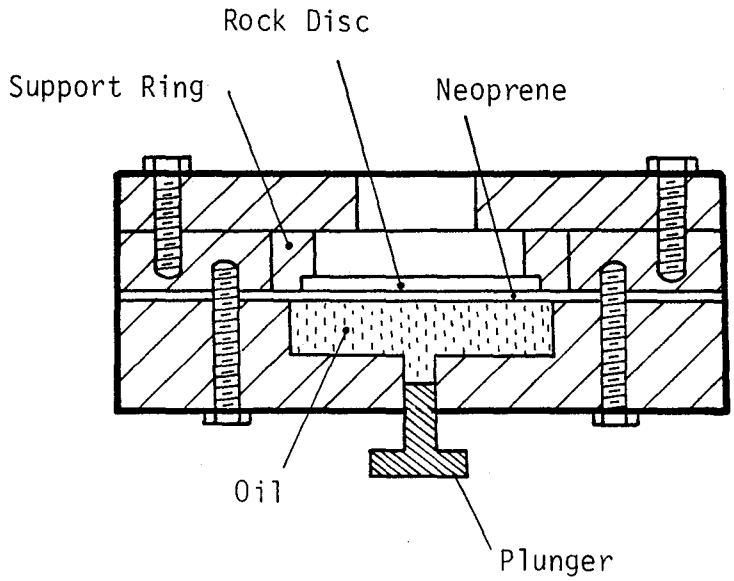

Figure 7-1a. Disc Bending Apparatus (After Swan (1980a)).

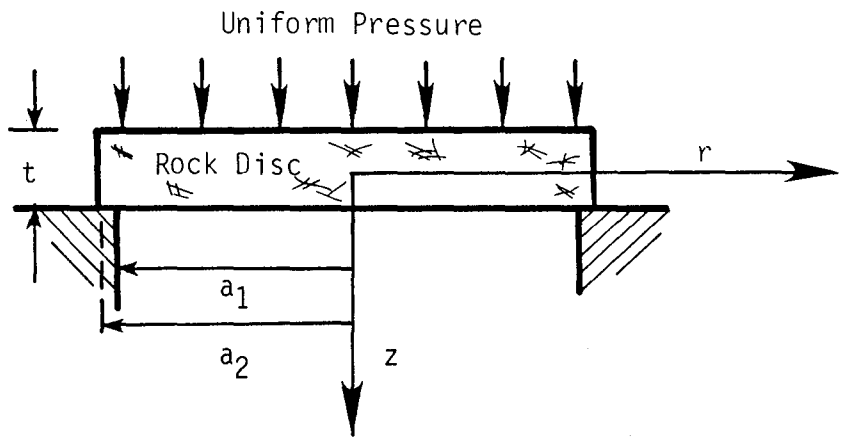

Figure 7-1b. Coordinates and Dimensions of Disc Bending Specimen (After Swan (1980a)).

APPENDIX A

Description of Rocks Tested

The purpose of this appendix is to provide a brief description of the rock types used in this research. In situations where more detailed descriptions are available in the literature, references are given.

A.1 STRIPA GRANITE

The Stripa Granite used in this research was obtained from core taken from the SBH-4 borehole near the Stripa Mine in Sweden (Doe *et al* (1981)). The rock is medium grained and the mineral composition is nominally (Olkiewicz *et al* (1979)):

Mineral	Volume %
Quartz	44
Feldspars	51
Muscovite	2
Chlorite	3

The accessory minerals are zircon and opaques.

The Stripa Granite contains extensive fissures, joints and fractures. The fractures are usually lined with chlorite and occasionally calcite (Olkiewicz *et al* (1979)). Many of the discontinuities are filled with epidote.

A.2 CARRARA MARBLE

The marble used in this research was obtained from the Oakland Granite and Marble company of Berkeley, California, and is believed by the suppliers to be Carrara Marble. This rock is for all practical purposes pure calcite with only a slight dark mineral structure observable in blocks of the order of 0.5 meter on a side . The Carrara Marble is medium-

to-fine grained and displays a distinct sugary texture. Carrara Marble has been tested extensively in the rock mechanics community (*e.g.*, Hoskins (1969)).

A.3 SIERRA WHITE GRANITE

The Sierra White Granite used in this research was obtained from the Oakland Granite and Marble Company. Sierra White Granite is a commercial name used by the supplier for a granodiorite extracted from the Raymond Quarry near Fresno, California.

This granodiorite is a white, medium grained rock with plagioclase content dominating over the potash feldspar. A dark biotite and green hornblende are the major accessory minerals. The minor accessory minerals are apatite, titanite and zircon. A detailed description of the regional rocks and geology of this area is given by Durrell (1936).

APPENDIX B

Risk of Rupture for Tension Tests

B.1 FOUR POINT BENDING

B.1.1 Volume Flaws

The risk of rupture for this test may be obtained by substituting the stress state from Equation (5-3) into the risk of rupture formulation of Equation (2-12). The stress state in each of the beam cross-sections (square, diamond and circular) is functionally identical. Therefore, the risk of rupture will only vary due to the domain over which the volume integral is taken. The form of the risk of rupture for four point bending of any beam cross-section can be shown to be;

$$B = \frac{V}{\pi}\left[\frac{T_a^{\,2}}{G_o}\right]^{\alpha} C_1 \int_{\frac{G_u^{1/2}}{T_a}}^{1} \int_{-\frac{\pi}{2}}^{\frac{\pi}{2}} \int_{-\frac{\pi}{2}}^{\frac{\pi}{2}} F_1^{\alpha}(\eta,\phi,\psi) + 3 \int_{\frac{1}{3}}^{\xi_o(\eta)} F_2^{\alpha}(\xi,\eta,\phi,\psi)\, d\xi \cos(\phi)\, d\phi\, d\psi\, H(\eta)\, d\eta \tag{B-1}$$

where:

C_1 = a constant dependent upon the beam cross-section

$H(\eta)$ = a function dependent upon the beam cross-section

ξ_o = limit of ξ where F_2 is positive.

The functions F_1 and F_2 are;

$$F_1 = \eta^2\cos^4(\phi)\cos^4(\psi) - \frac{G_u}{T_a^{\,2}} \tag{B-2a}$$

$$F_2 = \left[\frac{3\eta}{2}(1-\xi)\right]^2 \cos^4(\phi)\cos^4(\psi) - \frac{G_u}{T_a^{\,2}} \tag{B-2b}$$

The functions F_1 and F_2 are only defined in the positive domain. Negative values do not contribute to the risk of rupture formulation of Equation (B-1). The integration limits on ϕ and ψ could be adjusted to only consider positive values of F_1 and F_2; however, for computer programming purposes, it is more convienient to use a logical IF statement to disregard negative values of F_1 and F_2 and thus, retain the limits on ϕ and ψ given above (Pankow (1978)).

The values of C_1 and the form of the function $H(\eta)$ for each beam cross-section is given in Table B-1.

B.1.2 Surface Flaws

The risk of rupture for beams in four point bending assuming surfacially distributed defects is found by substituting the appropriate stress distribution on the surface into Equation (2-12). However, rather than performing the volume integration of Equation (2-12), a surface integration is performed. The form of the risk of rupture in this case can be shown

TABLE B-1

Parameters for Risk of Rupture
Four Point Bending-Volume Flaws

Cross Section	C_1	$H(\eta)$
Square	$\frac{1}{12}$	1
Circular	$\frac{1}{3\pi}$	$(1-\eta^2)^{1/2}$
Diamond	$\frac{1}{6}$	$(1-\eta)$

to be;

$$B = \frac{aL}{6\pi}\left[\frac{T_a^{\,2}}{G_o}\right]^{\alpha} C_1 \int_{-\frac{\pi}{2}}^{\frac{\pi}{2}}\int_{-\frac{\pi}{2}}^{\frac{\pi}{2}} F_1^{\alpha}(\phi,\psi)\; C_2 \;+\; \int_{\frac{G_u^{1/2}}{T_a}}^{1} F_2^{\alpha}(\eta,\phi,\psi)\, H(\eta)\, d\eta \qquad \text{(B-3)}$$

$$+\; 3\int_{\frac{1}{3}}^{\xi_o} F_3^{\alpha}(\xi,\phi,\psi)\; C_2\; d\eta + \int_{\frac{G_u^{1/2}}{T_a}}^{1} F_4^{\alpha}(\eta,\xi,\phi,\psi)\; H(\eta)\; d\eta\; d\xi \cos(\phi)\; d\phi\; d\psi$$

where:

$C_1,\ C_2$ = constants dependent upon the beam cross-section

$H(\eta)$ = a function dependent upon the beam cross-section.

The functions F_1, F_2, F_3, and F_4 which again are only defined in the positive domain are;

$$F_1 = \cos^4(\phi)\cos^4(\psi) - \frac{G_u}{T_a^{\,2}} \qquad \text{(B-4a)}$$

$$F_2 = \eta^2\cos^4(\phi)\cos^4(\psi) - \frac{G_u}{T_a^{\,2}} \qquad \text{(B-4b)}$$

$$F_3 = \left[\frac{3}{2}(1-\xi)\right]^2 \cos^4(\phi)\cos^4(\psi) - \frac{G_u}{T_a^{\,2}} \qquad \text{(B-4c)}$$

$$F_4 = \left[\frac{3\eta}{2}(1-\xi)\right]^2 \cos^4(\phi)\cos^4(\psi) - \frac{G_u}{T_a^{\,2}} \qquad \text{(B-4d)}$$

The values of C_1, C_2 and the form of $H(\eta)$ for each of the beam cross-sections are given in Table B-2.

TABLE B-2

Parameters for Risk of Rupture
Four Point Bending-Surface Flaws

Cross Section	C_1	C_2	$H(\eta)$
Square	1	1	1
Circular	1	0	$(1-\eta^2)^{-1/2}$
Diamond	½	0	1

B.2 LABORATORY HYDRAULIC FRACTURING

B.2.1 Volume Flaws

The risk of rupture for the laboratory hydraulic fracturing test is obtained by substituting the stress state for the configuration in Figure 5-6 (neglecting end effects) into the risk of rupture formulation of Equation (2-12). As mentioned in Chapter 5, the rock is assumed to be impermeable to the fracturing fluid. The resulting risk of rupture is;

$$B = \frac{V_h}{\pi}\left[\frac{T_a^{\,2}}{G_o}\right]^{\alpha} \int_1^{\frac{b}{a}} \int_{-\frac{\pi}{2}}^{\frac{\pi}{2}} \int_{-\frac{\pi}{2}}^{\frac{\pi}{2}} F^{\alpha}(\rho,\phi,\psi)\cos(\phi)\, d\phi\, d\psi\, \rho\, d\rho \qquad \text{(B-5)}$$

where:

V_h = volume of internal borehole

a = inner radius

b = outer radius

$$F = \frac{1}{T_a^{\,2}}\left[\sigma_n^{\,2} - G_u\right]$$

The normal stress, σ_n, for this case is defined as;

$$\sigma_n = \sigma_\theta \cos^2(\phi)\cos^2(\psi) + \sigma_r \sin^2(\psi) \qquad \text{(B-6)}$$

where:

$$\sigma_\theta = T_a \left[\frac{1 + \left(\frac{b}{\rho a}\right)^2}{1 + \left(\frac{b}{a}\right)^2} \right] \tag{B-7a}$$

$$\sigma_r = T_a \left[\frac{1 - \left(\frac{b}{\rho a}\right)^2}{1 + \left(\frac{b}{a}\right)^2} \right] \tag{B-7b}$$

As in the case of the four point bending, F is defined only in the positive domain, rather than evaluating the corresponding limits of integration on ρ, ϕ and ψ.

B.2.2 Surface Flaws

The risk of rupture for the laboratory hydraulic fracturing test assuming surfacially distributed flaws is obtained by substituting the stress state at the internal borehole wall into the risk of rupture formulation of Equation (2-12) and performing a surface integration rather than a volume integration. The risk of rupture is found to be;

$$B = \frac{A_h}{2\pi} \left[\frac{T_a^2}{G_o} \right]^\alpha \int_{-\frac{\pi}{2}}^{\frac{\pi}{2}} \int_{-\frac{\pi}{2}}^{\frac{\pi}{2}} F^\alpha(\phi,\psi) \cos(\phi)\, d\phi\, d\psi \tag{B-8}$$

where:

A_h = surface area of internal borehole.

The function F is defined in Equation (B-5). The normal stress σ_n for this case is defined as;

$$\sigma_n = T_a \cos^2(\phi)\cos^2(\psi) + T_a \gamma \sin^2(\psi) \tag{B-9}$$

where:

$$\gamma = \left[\frac{1 - \left(\frac{b}{a}\right)^2}{1 + \left(\frac{b}{a}\right)^2} \right]$$

As before, the function F is only defined in the positive domain.

B.3 RUBBER FRACTURING

The only risk of rupture for this test (with $G_u \neq 0$) which will be derived in this appendix is for the case where flaws are surfacially distributed. For this case, the contribution to the risk of rupture at the internal borehole surface will be neglected (see Chapters 5 thru 7). Substituting the stress state on the upper and lower surfaces of the rubber fracturing disk into the risk of rupture formulation of Equation (2-12) and performing a surface integration rather than a volume integration leads to;

$$B = 2a^2 \left[\frac{T_a^{\,2}}{G_o} \right]^{\alpha} \int_1^{\frac{b}{a}} \int_{-\frac{\pi}{2}}^{\frac{\pi}{2}} \int_{-\frac{\pi}{2}}^{\frac{\pi}{2}} F^{\alpha}(\rho,\phi,\psi) \cos(\phi)\ d\phi\ d\psi\ \rho\ d\rho \qquad \text{(B-10)}$$

The function F and the normal stress σ_n for this test are defined in Equation (B-5).

This report was done with support from the Department of Energy. Any conclusions or opinions expressed in this report represent solely those of the author(s) and not necessarily those of The Regents of the University of California, the Lawrence Berkeley Laboratory or the Department of Energy.

Reference to a company or product name does not imply approval or recommendation of the product by the University of California or the U.S. Department of Energy to the exclusion of others that may be suitable.

TECHNICAL INFORMATION DEPARTMENT
LAWRENCE BERKELEY LABORATORY
UNIVERSITY OF CALIFORNIA
BERKELEY, CALIFORNIA 94720